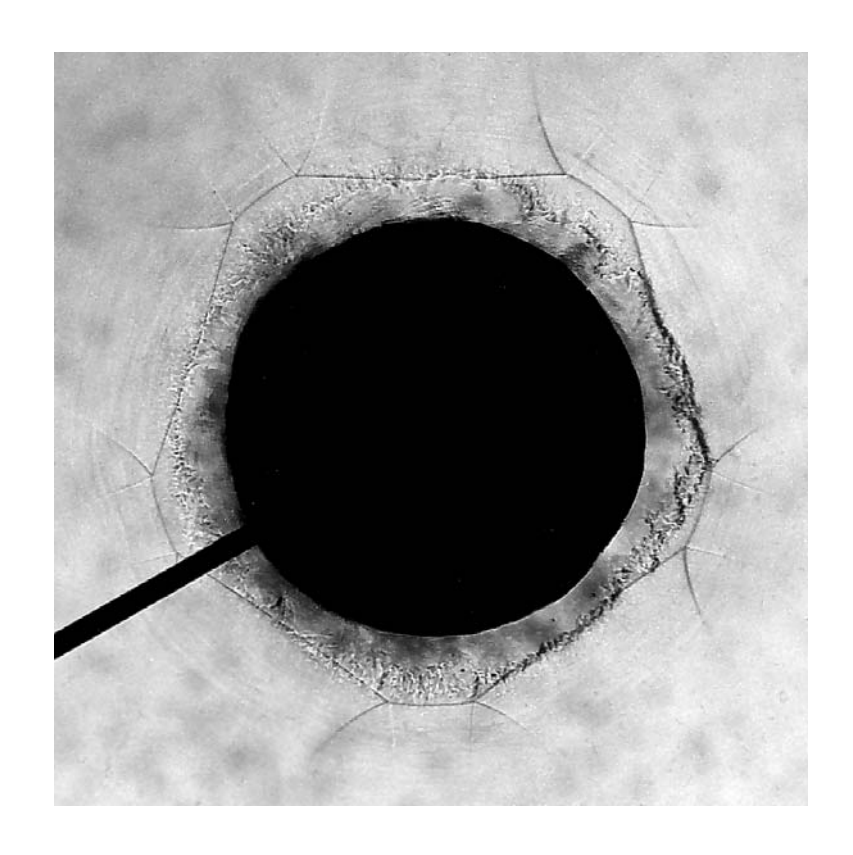
Experimental study of shock wave focusing in a confined reflector

Bo Johansson



Abstract

The main objective of the present work is to carry out experimental investigations concerning generation and focusing of polygonal shaped shock waves in a procedure introduced by Apazidis & Lesser (1996). In this procedure an expanding circular cylindrical shock wave with constant Mach number distribution along the shock front is generated at the center of a confined gas filled chamber. The chamber boundary has the form of a slightly perturbed circle. The shock reflects off the boundary and converges in the inner of the chamber into a polygonal shape. The polygonal shape of the shock undergoes a continuous change as the shock progresses in the inner of the chamber. This as a result of a coupling between the local curvature of the shock front and the speed of its propagation. For this experimental study, a chamber with a specific form of the boundary was designed and manufactured. Shocks were generated by means of an electrical discharge. A schlieren system with camera and flash device with time-delay, was used in order to visualize the process of shock propagation, reflection and convergence at various locations in the chamber. The speed of the shock was measured by means of two methods. Photographs with double exposures were used for the shock speed estimations in the case of weak shocks. For stronger shocks a laser beam system was utilized in determining the shock speed at various locations in the chamber and along the shock front. The experimental results of the current investigation confirmed the theoretical predictions obtained in earlier studies of similar problems. The major new result showed that it is possible to generate polygonal shaped shocks with sharp corners and plane sides by means of reflection from a smooth boundary. This particular shock formation is of importance since the evolution of the shock front in the corner area was observed to reproduce the major features of the nonlinear shock behaviour in the focal area. The present experimental study of the shock front evolution in the process of convergence also confirmed the earlier computational results. The latter indicating a complex behaviour of the converging shock front that stems from the highly nonlinear nature of the phenomenon due to the interaction between the local form of the shock and the speed of its propagation. The shock strength at the reflector boundary was in the range M = 1.1 - 1.7 increasing to M = 2.7 at the location close to the center of the chamber. The proposed experimental procedure showed to be a simple, stable, repeatable and reliable method to produce highly symmetrical polygonal-shaped converging shocks.

Contents

1	Int	roduct	ion	1
2	The	eoretic	al formulation	5
	2.1	The g	eneral idea, the chamber design and its basic function	5
	2.2	_	reflection	6
	2.3	Theor	retical methods of shock propagation	7
		2.3.1	The acoustic shock propagation, geometrical acoustics	7
		2.3.2	The non-linear propagation, geometrical shock dynamics	8
	2.4	Exam	ples of calculated results	11
		2.4.1	Acoustic shock propagation	11
		2.4.2	Strong shock propagation	12
3	Exp	\mathbf{erime}	ntal investigation	15
	3.1		imental apparatus	16
		3.1.1	The chamber construction	16
		3.1.2	Shock generating device	17
	3.2	The sl	hock visualization method	19
		3.2.1	The schlieren method	19
		3.2.2	Optical set-up	20
		3.2.3	Preparations of the optical set-up	20
		3.2.4	Light conditions and disturbing light reduction	23
	3.3	Time	control and measuring	24
	3.4	Shock	speed measurements	25
		3.4.1	The shock speed estimation system	25
	3.5	Exper	imental procedures	28
		3.5.1	Weak shock experimental procedure	28
		3.5.2	Moderate and strong shock experimental procedure	29
		3.5.3	Shock speed measurement procedure	31
4	Res	ults aı	nd comparison with theory	33
	4.1	Shock	speed estimation	34
		4.1.1	The speed of the weak shocks	34
		4.1.2	The speed of the moderately strong shocks	36
	4.2	The c	onverging shocks	42
		4.2.1	The weak shock propagation	42
		4.2.2	The moderately strong shock propagation	47
	4.3	Comp	parison with some theoretical results	55
5	Sun	nmarv	of the major results	63

ii	B. Johansson
Acknowledgement	64
References	64
Paper 1	

1 Introduction

There is a wide range of phenomena in nature involving shock waves. Sonic booms caused by thunders and supersonic aircraft are perhaps the most well known of these phenomenon. Explosions such as those from volcanic eruptions and atomic bomb explosions produce shock waves of immense strength causing great destruction. Shock waves do not only occur in these 'large scale' situations but are also present in situations of smaller scales. Erosion caused by impact between liquid drops and solids, (e.g. aircraft), is one area where the shock wave phenomenon plays a key role. Liquid drop impact has been studied thoroughly during the past decades. The research reveals the complexity of this problem area involving such features as e.q. high transient pressures and cavitation. Damage caused by cavitation is a well known but still an open issue. Recent research results indicate that a shock wave is generated as a result of the cavity collapse. The spectacular phenomenon of sonoluminescence during which the collapsing gas cavities in liquid emit a bright glow is also believed to be caused by shock wave focusing. Wherever shock waves occur spontaneously they seems to be connected to destruction and loss of energy.

In man's keenness to harness the forces of nature, shock waves have nowadays become partners in the mankind's service, where the destructive behavior of shock waves has found its place in certain technical applications. Extracorporeal shock wave lithotripsy (ESWL), i.e. disintegration of kidney and bladder stones by focusing ultra sound that transforms into a shock is an important field that already has changed the method of treatment, where the need for surgery has decreased. Another technical application is focusing of shock waves to produce high speed water jets, applicable in deliberate cutting of hard solids, surfaces cleaning and erosion testing of materials. A certain method to produce these water jets is by using a water-filled chamber of an elliptical geometry where a shock is produced in one of the focal points and by reflection from the elliptical boundary the shock is focused at the second focal point. The focusing process gives rise to a large pressure that can be utilized to produce a water jet. Investigations of this special technique were performed by Gustafsson (1985, 1987) who studied the problem theoretically by using perturbation theory and geometrical acoustics, and in experiments carried out in a water filled cavity. The results of this investigation show that the constant pressure distribution of the initial diverging shock changes after reflection off the cavity boundary to a non-homogeneous pressure distribution along the converging shock front. An extended quasi three-dimensional analysis of the problem based on geometrical acoustics was introduced by Apazidis (1992). In this investigation it is shown that a desired pressure

distribution can be obtained by an appropriate choice of the upper surface of the cavity.

The above examples describe phenomena and technical applications where shock waves occur. The special topic of the shock wave focusing studied experimentally in the present work should not be considered as a specific and isolated example. In fact, the results of the present study indicate that the features of the phenomenon studied here are common for the process of shock wave focusing in general. The shock wave focusing in itself is a common process and occurs as a result of a shock wave reflection off a concave surface. The geometry of a closed cavity does always include at least one concave surface which means that if a shock wave is present inside the cavity it will be focused after reflection off the cavity boundary.

In the experimental investigation by Sturtevant & Kulkarny (1976) the focusing processes of plane shocks reflected off a slightly parabolic reflector was studied. This study considered focusing of shock waves in the range from acoustic to moderately strong shocks. The main result of this study shows that the behaviour of a converging shock front in the vicinity of the focal region is governed by the shock strength. Acoustic or very weak shocks were observed to focus in the vicinity of a focal point. In case of stronger shocks a different focusing pattern was observed with a formation of a focusing region in which the shock fronts were 'flattened' and propagated in a certain well defined manner. This experimental study illustrated a highly complex nonlinear behaviour of shock waves in the focusing region. Some features of this process were described in the theoretical work of Schwendeman & Whitham (1987) which was based on Whitham's theory of Geometrical Shock Dynamics, GSD, Whitham (1957, 1959). They showed that a converging shock wave of an initial perturbed polygonal shape with smooth corners, will focus into a real polygon with sharp corners. However, Schwendeman's & Whitham's theoretical work does not suggest how to generate such an initial shock front.

In the theoretical investigation by Apazidis & Lesser (1996) a procedure to study the focusing processes of shock waves of arbitrary strength was introduced. In this procedure an outward propagating circular cylindrical shock wave is reflected off a confined reflector boundary of a specific geometrical form. The process of propagation reflection and convergence of such shock is studied in detail. This investigation is also based on Whitham's theory. In this theory the shock propagation is described by means of a nonlinear model in which the form of the shock is coupled to the local speed of the shock front. One of the assumptions of this theory is based on the fact that the shock propagates into a non-perturbed region with no flow ahead of the shock. In Whitham (1968) a modified version of GSD was introduced that takes into

account the influence of a uniform flow ahead of the shock front. In this version Galilean invariance is used to transform the equations of GSD to a reference frame fixed to the oncoming flow. Neither of these conditions are fulfilled in the present situation, since the converging shock will propagate into a region with a non-uniform flow field created by the outgoing cylindrical shock. Whitham's theory was therefore extended by Apazidis & Lesser (1996) to account for the non-uniform flow conditions ahead of the propagating shock. Computations based on this extension of Whitham's method were then performed in the case of a thin cylindrical chamber with a specific form of the boundary. The boundary - a slightly perturbed circle of a polygonal shape, with smooth well rounded corners, was chosen deliberately. In these calculations a numerical so called 'leap frog scheme' introduced by Henshaw et al. (1986) is used to propagate the converging shock. The computational results showed that a cylindrical shock with a constant Mach number distribution will after reflection off such a boundary transform into a shape with smooth corners that is close to the shape of the reflector boundary. As the shock will converge into the inner of the chamber its form will not be sustained but will undergo a continuous transformation. This transformation in the shape of the shock is due to the inherent nonlinearity of the process of shock propagation which stems from the nonlinear coupling between the local shape of the shock and the local speed of its propagation. The nonlinear mechanism results in an immensely increased curvature of the shock front corners that transforms the smooth shock form into a pure polygonal shape with plane sides and sharp corners. This increases the propagation speed of the shock in the corner regions due to the nonlinear coupling mechanism between the local curvature of the shock front and the speed of its propagation. Points on the shock front in the corner region will thus propagate in the inner of the chamber with a speed which is higher than the speed of propagation of a neighboring flat portion of the shock resulting in a transformation of the shock shape in accordance with a well defined scheme. The procedure to study focusing processes introduced by Apazidis & Lesser (1996) constitutes the basis for the present experimental investigation.

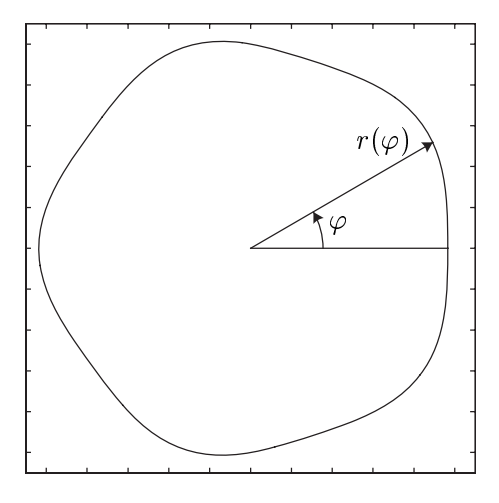


Fig. 1. Reflector boundary geometry.

2 Theoretical formulation

2.1 The general idea, the chamber design and its basic function

The chamber boundary suggested by Apazidis & Lesser is given in parametric form by the equation

$$r = \frac{1}{1 + \epsilon \cos(n\varphi)}. (1)$$

In figure 1 a reflector boundary with n=5 and $\epsilon=0.035$ is shown, (the boundary geometry used in the present work). What does then motivate this special boundary design? It is well known that a reflection of a circular weak shock at a parabolic boundary will result in a plane wave. This is also true for stronger shock waves but only for a short distance of propagation after the reflection. Since the present boundary in the regions around the maxima and minima is approximately parabolic, it is expected that the wave form will tend to become plane about these points. This seems to be a promising line of argument in creating polygonal shaped shock waves with plane sides. One can ask why the choice of five corners for the experiments why not four or six corners instead and the answer to this comes from the calculations made by Apazidis & Lesser (1996). With a boundary having four corners the shock focusing areas appears too close to the chamber center and with six corners the focusing areas seems to be too close to each other. The appropriate choice of corners seems to be five according to the theoretical results.

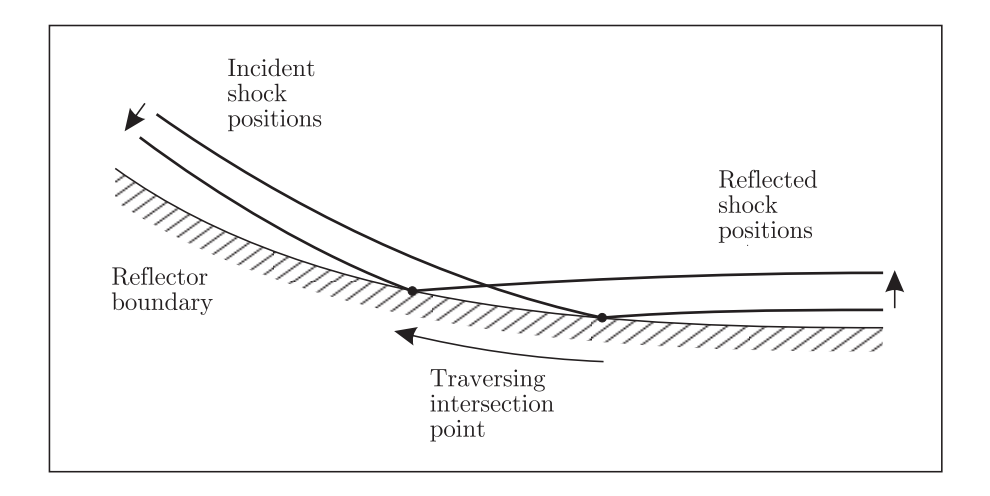


Fig. 2. The reflection point traversing the boundary.

2.2 Shock reflection

The theoretical analysis of the problem starts at the moment when the circular outward propagating shock front reaches the positions of the smallest radius of the boundary, the first five points of intersection. At these points a reflection process starts that continues during a time in which the whole reflector boundary is traversed by the outward propagating shock front. A sketch of a shock traversing a curved boundary is shown in figure 2. The incident shock traverses the boundary at a moving point and reflects off the boundary.

When a moving shock wave reaches a solid boundary it reflects in a way that depends on the local shock strength and the angle of incidence. The relations between the incoming wave and the reflected one is governed by the same relations used for a stationary oblique shock reflected at a solid boundary. For a detailed discussion concerning the theoretical approach and the relations see e.g. Anderson (1990). A sketch of a shock reflection is shown in figure 3. If we consider a reference frame attached to the point of intersection, the shock experiences an oncoming flow as shown in figure 3. The reflected shocks are viewed from a reference frame in which they are stationary, that is why the relations also apply to this case. (One can ask whether the reflection relations holds also for curved shock waves? If we look at a small area around the point of intersection the answer to this question is yes.)

Three regions with different flow conditions are obtained which are related to each other by the shock reflection relations. The normal component of the Mach number M_{2n} in region 2 is related to the incident Mach number M_i in

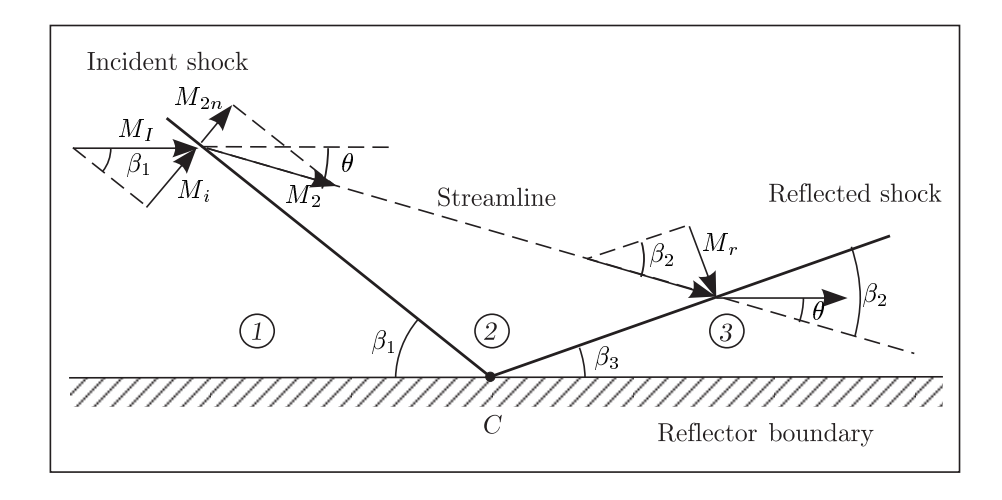


Fig. 3. Reflection of an incoming oblique shock from a solid boundary.

region 1 by the normal shock relation. The deflection angle θ is then obtained from a θ - β -M relation with the angle of incidence β_1 and the incident Mach number M_i . Then the Mach number M_2 is given by a trigonometric relation. The θ - β -M relation is used again to derive the angle β_2 . Trigonometric relations then gives the reflected Mach number M_r as well as the angle of reflection β_3 . From this it is easy to find the normal direction to the reflected wave front n_r . This procedure provides an algorithm for calculating the reflected shock parameters when it sweeps the boundary.

2.3 Theoretical methods of shock propagation

2.3.1 The acoustic shock propagation, geometrical acoustics

The method of geometrical acoustics provides a simple solution of acoustic discontinuity problems and can also give some qualitative results to certain problems with week shocks. In the method of geometrical acoustics 'rays' are introduced defined as orthogonal trajectories of the successive positions of the shock front. The idea is to propagate each element of the shock front through a 'ray-tube'. A ray-tube can be considered as a ray surrounded by a wall of neighboring rays. For geometrical acoustics the propagation is a rather simple procedure this since the rays are all straight lines orthogonal to the shock front. The reasons why the rays are straight lines is due to the assumption of a constant shock speed equal to the speed of sound and that the conditions ahead of the shock is assumed to be quiescent. The special problem that is treated in the present investigation does also include reflection from a curved surface. For an acoustic shock the reflection angle

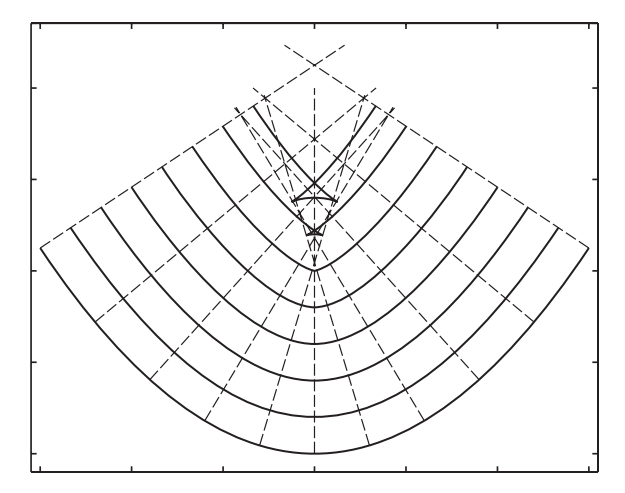


Fig. 4. Propagation of a parabolic wave front according to geometrical acoustics, wave fronts (solid), rays (dashed).

equals the incident angle and the Mach number of the reflected shock front equals that of the incident shock front. These conditions are consistent with the reflection relations described above.

In geometrical acoustics the pressure amplitude in first approximation can be shown to be proportional to the inverse of the square root of the ray-tube area. When a concave shock front is propagated along straight rays normal to the shock front the rays will eventually cross each other at certain points. This means that the ray-tube area at these locations goes to zero and consequently the pressure amplitude goes to infinity which gives a wrong picture of the physical reality. As a result of the crossing rays a crossing of the shock itself appears and the so called caustics are created. Caustics have been observed in experiments with weak shocks which indicates that geometrical acoustics is a reasonable model for these types of flows. In the calculations shown in the figure 4 an initially parabolic shaped shock front (solid lines) of constant speed is propagated along rays (dashed lines). The rays cross each other and the caustics of the shock are formed. The surface on which adjacent rays cross is called a caustic surface. More information about geometrical acoustics can be found in e.g. Whitham (1974), (geometrical optics).

2.3.2 The non-linear propagation, geometrical shock dynamics

Geometrical shock dynamics (GSD) developed by Whitham (1957), is an approximate geometrical non-linear theory for propagation of shock fronts. The method extends the ideas of geometrical acoustics where each element

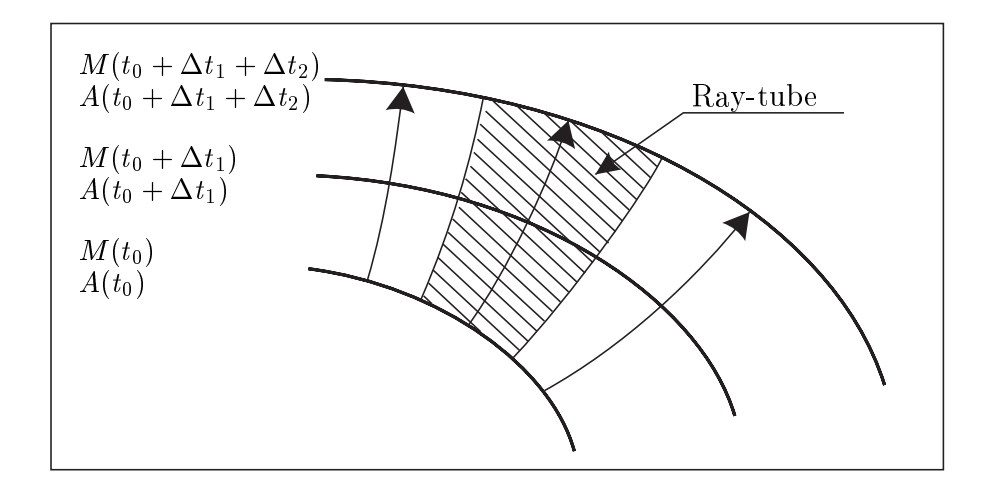


Fig. 5. Shock front positions at different instants. Rays and ray-tube.

of the shock front is propagated with a constant speed equal to the speed of sound through a 'ray-tube'. In GSD the speed of propagation along a ray depends on the Mach number at each location and the propagation down a ray-tube is governed by a relation between the ray-tube area and Mach number an A-M relation, see figure 5. This provides a method to take care of discontinuities in the shock front by accelerating the locations of large curvature, which assures that the shock strength does not go to infinity at these locations.

The governing equations for geometrical shock dynamics are the quasione-dimensional equation of mass conservation derived from the integral form of the mass conservation, the one dimensional momentum equation without the viscous term and the energy equation written in a special form for polytropic conditions, (polytropic equals a ideal gas with constant specific heats). These equations are

$$\rho_t + u\rho_x + \rho u_x + \rho u \frac{A'(x)}{A(x)} = 0, \qquad (2)$$

$$u_t + uu_x + \frac{1}{\rho}p_x = 0, (3)$$

$$p_t + up_x - a^2 \left(\rho_t + u\rho_x \right) = 0. (4)$$

From these equations the characteristic equation for the C_+ characteristic can be derived that is

$$\frac{dp}{dx} + \rho a \frac{du}{dx} + \frac{\rho a^2 u}{u+a} \frac{1}{A} \frac{dA}{dx} = 0.$$
 (5)

The equation 5 with the shock conditions

$$u = a_0 \frac{2}{\gamma + 1} \left(M - \frac{1}{M} \right),$$

$$p = \rho_0 a_0^2 \left(\frac{2}{\gamma + 1} M^2 - \frac{\gamma - 1}{\gamma (\gamma + 1)} \right),$$

$$\rho = \rho_0 \frac{(\gamma + 1) M^2}{(\gamma - 1) M^2 + 2}$$
(6)

inserted gives the relation between the ray-tube area and the Mach number as

$$\frac{M}{M^2 - 1}\lambda(M)\frac{dM}{dx} + \frac{1}{A}\frac{dA}{dx},\tag{7}$$

where

$$\lambda(M) = \left(1 + \frac{2}{\gamma + 1} \frac{1 - \mu^2}{\mu}\right) \left(1 + 2\mu + \frac{1}{M^2}\right),\tag{8}$$

$$\mu^2 = \frac{(\gamma - 1)M^2 + 2}{2\gamma M^2 - (\gamma - 1)}. (9)$$

The constant γ is the ratio of the specific heats. An alternative form is to write the A-M relation as

$$A = A_0 \frac{f(M)}{f(M_0)},\tag{10}$$

with

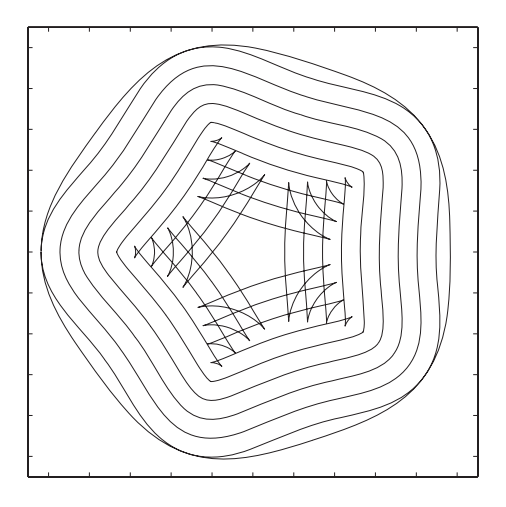
$$f(M) = \exp\left(-\int \frac{M}{M^2 - 1} \lambda(M) dM\right). \tag{11}$$

In 2-D the shock front positions r(x, y) is related to the A-M relation by a system of non-linear equations,

$$\frac{d}{dt}\mathbf{r}(t) = M(t)\mathbf{n}(t) \tag{12}$$

where n is normal to the shock front. This system together with the A-M relation provides a complete set of equations for evaluation of the shock front position and strength as a function of time. For more information about GSD, see Whitham (1974).

The standard version of GSD is however not able to deal with the influence of flow conditions ahead of the shock on the shock propagation. In



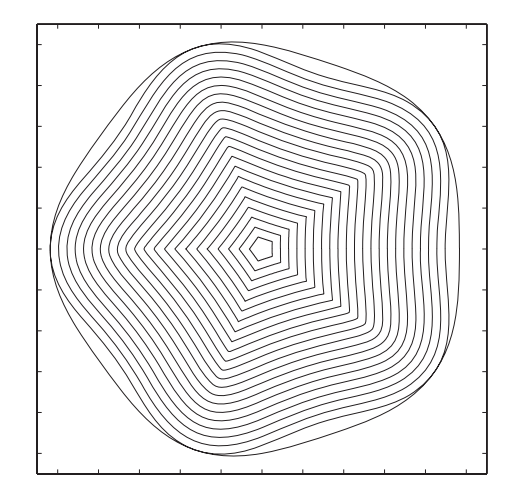


Fig. 6. Calculations according to geometrical acoustics.

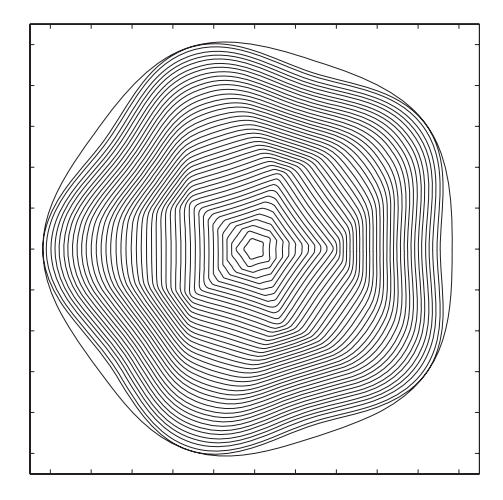
Fig. 7. Non-linear calculations at $M_0 = 1.01$, geometrical shock dynamics.

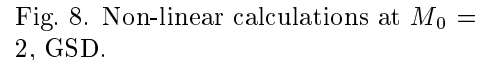
Whitham (1968) a modified version of GSD is introduced to deal with uniform conditions ahead of the shock front. In this version Galilean invariance is used to transform the equations of GSD to a reference frame fixed to the oncoming flow. As a result of this it is shown that the ray-tubes are not orthogonal to the shock-surface anymore. To develop equations for non-uniform flow conditions, which is the case in the present problem, Apazidis and Lesser followed a similar idea. This will work since the shock is merely a surface of discontinuity that has no mass. It is then possible to use a 'local' Galilean transformation to derive suitable equations of motion. The main contribution of this extension to Whitham's formulation is that new terms in the equations appear because of the gradient in the flow conditions. Also in this case the ray-tubes are not orthogonal to the shock-surface.

2.4 Examples of calculated results

2.4.1 Acoustic shock propagation

For an acoustic shock the shock strength is uncoupled with the shock speed which is always equal to the speed of sound and the direction of propagation is always in the normal direction to the shock front. In a situation where shock reflection occurs the convergence is totally determined by the initial shock form and the geometry of the reflector boundary. The figure 6 shows a calculation according to geometrical acoustics for the present boundary geometry. After the reflection the shock has a smooth shape that reminds of the boundary geometry itself. At a later stage the shock front 'corners' becomes sharp and a pentagon shaped shock front is formed. At this points





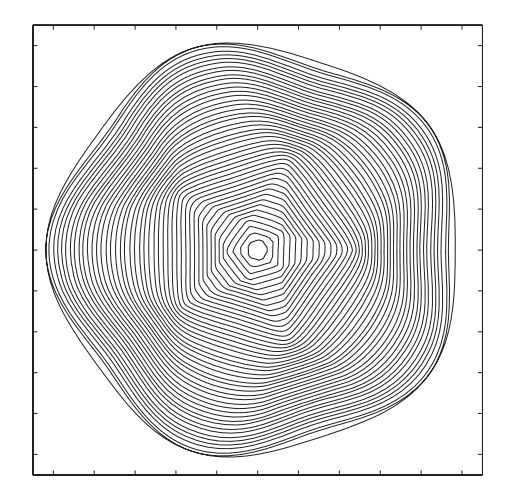


Fig. 9. Non-linear calculations at $M_0 = 5$, GSD.

a crossing of rays appears and consequently also a crossing of the shock itself. Now the formations of the so called caustics occurs, the sides of the triangular shapes. As will be shown in the results in section 4 these triangular shapes do appear in the weak shock case.

In the figure 7 a calculation based on the non-linear theory of geometrical shock dynamics is shown. The initial Mach number in this calculation is close to one M=1.01 and the flow conditions in front of the reflected shock is taken to be quiescent. In these calculations the triangular shapes of the caustics do not occur due to the acceleration of the shock front with high curvature.

2.4.2 Strong shock propagation

For strong shocks the non-linear mechanism of the wave propagation gives a completely different result than for the acoustic or weak shocks this since the flow ahead of the reflected shock can not be neglected. In the figures 8 and 9 from Apazidis & Lesser (1996) calculations at to different initial Mach numbers $M_0 = 2$ and $M_0 = 5$ are shown. In these calculations the propagating shock front are seen to form into a pentagon shape but in contrast to the weak shock calculations shown in the figures 6 and 7 the corners arise at positions located towards the chamber sides. During the continuation of the propagation the corners are seen to flatten out and after that a new pentagon shape is formed. The position of the corners alternates between being in the symmetric position of the chamber 'corners' or chamber 'sides' and this rotating or oscillating behaviour continues all the way into the center

of the chamber. The traces that are seen are called shock-shocks and arise from discontinuities in the shock front. For a larger initial Mach number the shock-shocks will show up earlier than for a smaller initial Mach number, compare the figures 8 and 9. Also in case of the flow ahead of the shock, the shock approaches the polygonal form at a position which is closer to the reflector boundary.

Although the form of the converging shock evolves even in the weak shock case it does not exhibit the complex oscillating behaviour as the one discussed above. In this case the shock forms into a pentagon and this shape is mainly preserved at all locations in the chamber.

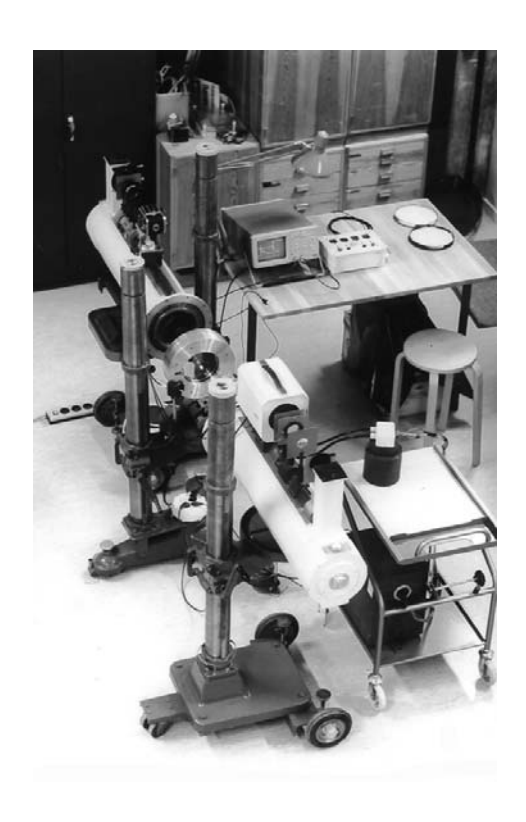
The computational method used in the above calculations is based on a numerical scheme introduced by Henshaw *et al.* (1986). In this method a two-step leap-frog scheme is applied to the equations 12

$$\boldsymbol{r}_{i}\left(t+\Delta t\right) = \boldsymbol{r}_{i}\left(t-\Delta t\right) + 2\Delta t M_{i}\left(t\right) \boldsymbol{n}_{i}\left(t\right), \ i=1,...,N,$$
(13)

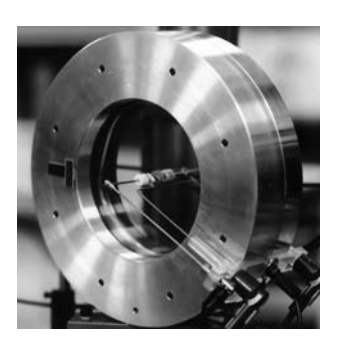
where the time-step is given by a certain stability condition. This gives the new positions of the shock front from which the corresponding ray-tube areas and propagation directions are derived. Then the Mach numbers are obtained from the A-M relation, equation 10. In the present calculations, due to the non-uniform conditions ahead of the shock, the directions of the propagation is not orthogonal to the shock front.

3 Experimental investigation

In the theoretical investigation by Apazidis & Lesser (1996) a procedure to study the focusing processes of shock waves of arbitrary strength was introduced. In this procedure an outward propagating circular cylindrical shock wave is reflected off a confined reflector boundary of a special geometrical form. The focusing process of the reflected inward propagating shock wave is studied and the shock front is seen to form into a polygonal shape. This procedure constitutes the basis for the experiments described in the present work. To perform the experiments, a thin cylindrical chamber with the desired boundary was designed and manufactured. The chamber was filled with gas at atmospheric pressure and the shocks were generated in the center of the chamber by means of two methods utilizing electrical discharge. The process of shock propagation, reflection and convergence was visualized with the help of a schlieren system, a camera and a flash light source, this together with the equipment for time-delay control and measurement. Weak shock



(a) The schlieren system.



(b) The chamber.



(c) The reflector plate.

Fig. 10. Experimental set-up.

speed estimations was made by utilizing double exposed photographs from which a mean speed of the shock could be derived. To estimate the shock speed for stronger shocks a time measuring system was built consisting of a laser beam mirrored twice through the chamber at positions located in the radial direction of the chamber. When a shock wave passes the positions of the laser beam the light is deflected and the event is registered by a photo diode connected to an oscilloscope.

3.1 Experimental apparatus

3.1.1 The chamber construction

A sketch of the chamber construction is shown in figure 11. The chamber is built up around the reflector plate, a circular plate made of aluminum with the desired reflector boundary milled out, see figure 12. Tracks in the reflector, made for O-ring gaskets that prevent leak in the joints between reflector plate and glass plates, were turned out. The glass plates are made of ordinary float glass and are provided with small center holes for insertion of the shock-generating device. The thickness of the glass plates is $15\,mm$. Two circular symmetric aluminum blocks enclose the inner plates. The blocks are tightened by eight M8 screws, and press via thick rubber O-rings the inner plate package together. The exterior dimensions of the chamber are: diameter $300\,mm$ and thickness $80\,mm$.

The usage of rubber O-rings between the aluminum blocks and glass plates gives a tolerable uniform pressure distribution that prevents the glass plates from cracking. This is of special importance if the experiments are performed in liquid since the pressure rise across the shock will become much larger than in experiments performed in gas. However, the present experi-

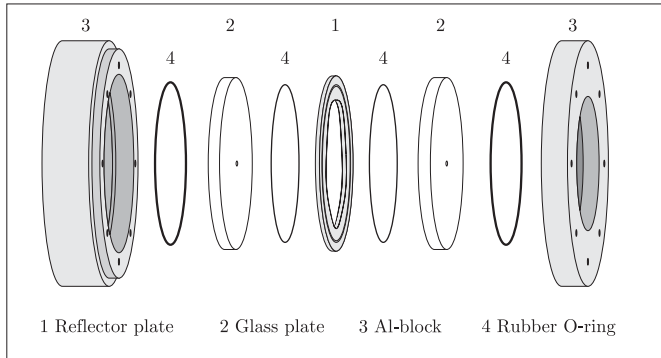




Fig. 11. The chamber construction.

Fig. 12. The reflector plate.

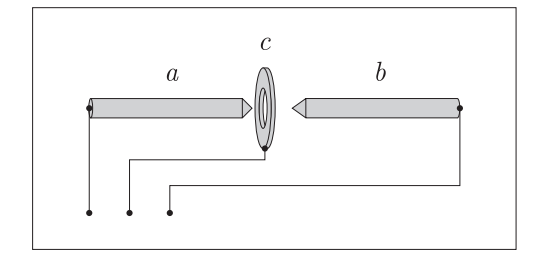
ments where performed in gases since the speed of sound in gases is much lower than in fluids which gives a larger resolution of the time scale. The gases used in the present study were air and argon with the speeds of sound $340 \, m/s$ and $318 \, m/s$ respectively. In the experiments with argon one of the glass plates was provided with a nipple for connection to the argon gas tube.

The maximum radius of the reflector boundary was set to $80 \, mm$, which is within the radius of the parallel beam in the schlieren system described below in section 3.2.2. The thickness of the reflector has to be considered in this respect. We can not expect the initial shock to be cylindrical, but if the thickness of the reflector is small compared to its radius the shock will change into an almost cylindrical shape. However, if the thickness is too small problems with boundary layers in the flow behind the shock may occur. Estimates made on the basis of dimensional analysis show that a thickness of some mm will be sufficient to avoid these problems. With the above criteria in mind the reflector thickness was set to $5 \, mm$.

3.1.2 Shock generating device

Shock waves can be produced in different ways, electrical discharge and explosives are some methods to be mentioned. Electrical discharge was used by Gustafsson (1985) in his experimental work with weak shock waves in an elliptical cavity. An electrical discharge gives rise to a sudden increase in temperature of the surrounding gas and consequently an increase in pressure that forms a propagating shock structure. At the initial stage the shock wave is not two dimensional but if the cavity is thin the shock will adapt the two dimensional form at a later stage. Depending on the shape of the boundary adjacent to the discharge zone the initial shock wave will become more or less symmetric in shape and the Mach number distribution may also vary along the shock front. In the present work two devices based on electrical discharge were used to produce shock waves in the chamber. These devices are both working with high voltage charged capacitors but there is a difference in the technique to trigger the discharge, in the way of overcoming the breakdown voltage in the spark gap.

The first discharge device is limited to produce weak shock waves and is based on an *igniting spark* technique. This method requires three electrodes, two main electrodes and one ignition electrode, see figure 13. One of the main electrodes a together with the ring formed ignition electrode c are inserted through one of the chamber glass plates, and the second main electrode b is inserted through the other glass plate. The gap distance between the main electrodes was about $4\,mm$. The main electrical circuit consists of an adjustable voltage up to $5\,kV$, charging a capacitor package of total $0.3\,\mu F$.



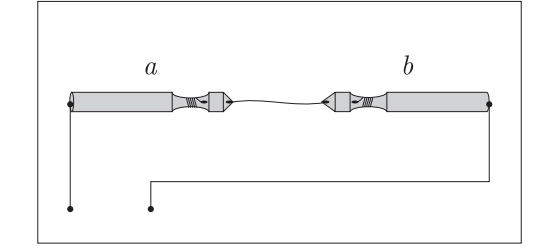
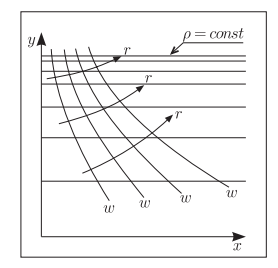


Fig. 13. Electrodes: Igniting spark.

Fig. 14. Electrodes: Exploding wire.

The capacitors are connected to the electrodes a and b. In the igniting spark technique a high voltage pulse is produced that overcomes the breakdown voltage in the gap between the two electrodes b and c. The spark opens up an ionized corridor in the gas that makes the main discharge to take place. The main electrodes are made from ordinary TIG, (Tungsten Inert Gas), welding electrodes and have a diameter of $2.4 \, mm$. These electrodes were provided with coned ends to secure a tolerable centering of the spark. The ring shaped ignition electrode is made of steel and has an outer and an inner diameter of $6 \, mm$ and $2.4 \, mm$ respectively.

The second discharge device was used to produce stronger shock waves and consists of a capacitor connected to two main electrodes via a triac. A triac can be described to be consisting of two parallel thyristors oriented in opposite directions. The triac opens up whenever the gate pulse has a positive or negative voltage. To overcome the breakdown voltage in the gap between the electrodes a so called *exploding wire* technique is used. Before each attempt a thin copper wire is placed between the two electrodes which in this case are suited for attachment of a thin wire, see figure 14. The main electrodes are made from the same TIG welding electrode material as the one used for the first device. The size of the capacitor is $33.5 \mu F$ and it is charged by an adjustable voltage from $1.4 \, kV$ to $3.4 \, kV$. A certain appliance is used to give a gate pulse to the triac that triggers the discharge. The thickness of a wire is about $0.05 \, mm$ and in the present experiments the length of the wires was adjusted to about 12 mm, i.e. the distance between the electrodes is larger than the reflector thickness which means that the wire ends are located inside the holes of the glass plates. Experiments with different wire lengths showed that a longer wire gives a stronger shock than a shorter wire and that the shock strength variation related to the wire length variation is less for a longer wire.



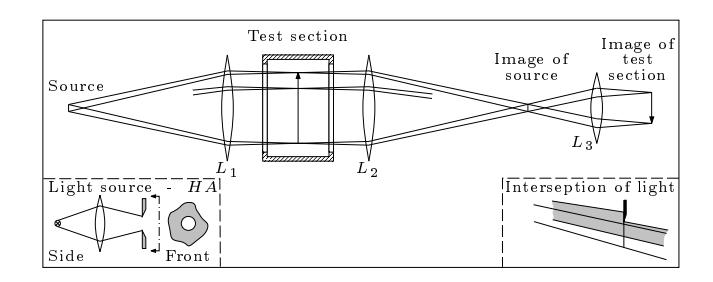


Fig. 15. Refraction in density field. Rays (r) and wave fronts (w).

Fig. 16. The schlieren system.

3.2 The shock visualization method

3.2.1 The schlieren method

The schlieren optical method depends on the fact that the speed of light and consequently the index of refraction vary with the density of the medium through which it is passing. Light that passes through an inhomogeneous gas, for instance a region of compressible flow, is because of the density gradient diffracted, see figure 15. In a schlieren system this diffraction is used to visualize for example a shock. The basic idea of the schlieren system is that a part of the deflected light is intercepted before it reaches the viewing screen or photographic plate. As a consequence of that, a region with inhomogeneous gas will appear darker than the surroundings. Regions lighter than the surroundings may also occur since some of the non-diffracted light may be intercepted while some of the diffracted light may pass the interception point, this depending on what interception method is used.

The details about the schlieren method can be found in e.g. Liepmann & Roshko (1957) but a short description is given below. A schematic description of the schlieren method is shown in the figure 16. In the left edge view the light source is shown. It consists of a hole aperture HA placed at the focus of a lamp-lens combination. By passing the light from the source through a lens L_1 , placed at the distance of its focal length from the hole aperture, a beam of parallel light is obtained. The light beam passes through the test section and continues through a second lens L_2 that focuses the light. Two different image planes are seen where the first is the image plane of the light source that is located at the focal point of the lens L_2 . At the second plane the image of the test section is located. The image of the light that is deflected at the position of the test section will be focused adjacent to the focal point of the non-deflected light. This means that we can intercept some of the deflected light at the position of the light source image to prevent the

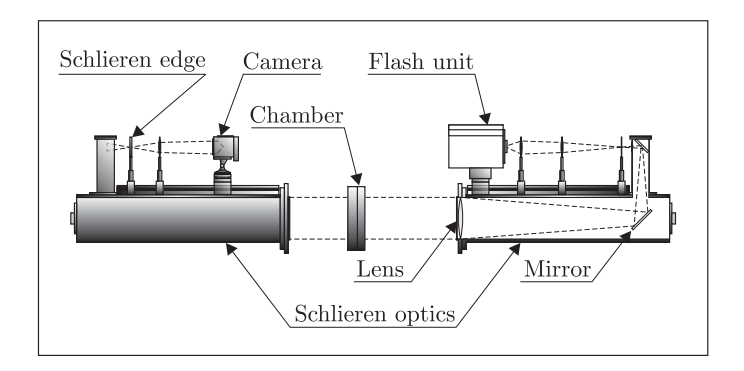


Fig. 17. The optical set-up.

deflected light from reaching the image plane of the test section, see the right edge view.

3.2.2 Optical set-up

In the present work an existing schlieren system was used, consisting of two equivalent optical appliances used for light source respectively image application, see figure 17. An optical appliance mainly consists of a large lens which has a diameter of 185 mm and a focal length of 1310 mm. Inside each appliance there are two mirrors that turn the light into a section located at the top of the appliance. Along this section a metal girder for attachment of other equipment in the optical set-up is mounted. By passing the light from the light source through the focal point of the first schlieren lens and through the lens, a beam of parallel light is obtained. The light beam goes through the test section and continues through the schlieren lens of the second appliance that focuses the light. A schlieren edge put at the position of the focal point of this lens intercepts some of the deflected light before it reach the camera. As a schlieren edge a razor blade can be used.

In the procedure to record the experimental course of events a camera with open shutter and a flash unit provided with two inputs for single or double flash, was used. The camera was a Hasselblad 1000f provided with an ordinary camera back and an extra Polaroid camera back. Three lenses, hole aperture and polarization filters were the other parts in the optical set-up.

3.2.3 Preparations of the optical set-up

An accurate adjustment of all different components in the optical set-up is crucial for the experimental outcome. These adjustments can be a somewhat time consuming but it is worthwhile to spend some extra hours with that.

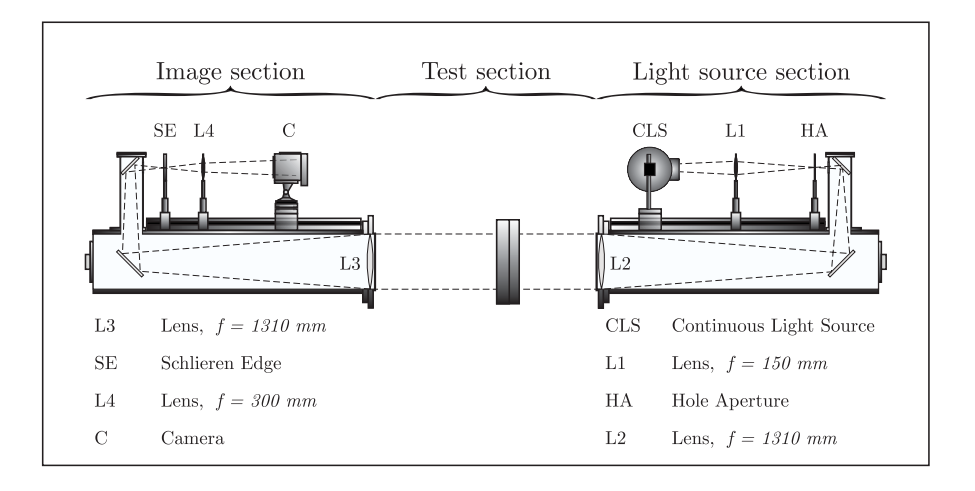


Fig. 18. The optical components.

The procedure begins with adjustments of the components in the light source section, this to derive a parallel beam in the test section, see figure 18. The next step is to align the two schlieren appliances. After that the components in the image section are adjusted in order to obtain a sharp image of the chamber. The last stage in the procedure is to adjust the schlieren light interception. A more detailed description of the adjustment procedure follows below:

- The preparations of the optical set-up begin with an adjustment of the light source section in order to obtain a parallel beam through the test section, see figure 18. Initially the light source section consists of a continuous light source CLS, one lens L1 and a hole aperture HA placed on top of a schlieren appliance. As a first measure the hole aperture is positioned as close as possible to the focal point of the schlieren lens L2. Then the positions of the light source and the lens L1 are adjusted so that the light is focused at the hole aperture. The light goes through the hole aperture and continues trough the lens L2 which deflects the light into a parallel beam. The parallel beam is obtained by a correct adjustment of the hole aperture position to the focal point of lens L2. This is done by putting a plane mirror close to and perpendicular to the lens L2, then the light is mirrored back and focused on the hole aperture. If the position of the hole aperture is correct the focal point of the reflected light will have almost the same size as the hole aperture which means that the light that comes out of lens L2 into the test section is parallel.
- · When the light in the test section is parallel it is time to align the two schlieren appliances. Both appliances are placed on machine stands pro-

vided with wheels and adjustable supports to the floor. The machine stands are also adjustable in vertical and rotational positions. The six degrees of freedom make it possible to adjust the appliances in all directions. A correct alignment is achieved when the parallel beam is fit to the lens L3 and the resulting focal point is correctly positioned in the image section.

- The next step is to derive a sharp image on the viewing screen of the camera. The sharpness adjustment is preceded by calculations to obtain approximate positions of the chamber, the lenses and the camera respectively. In these calculations the size of the image is prescribed. Usually these calculated positions need to be adjusted afterwards. This is made by putting a hair on the chamber glass plate and move the camera C and the lens L4 along the metal girder until a good sharpness is obtained.
- · Adjustment of the schlieren interception position is performed by moving the schlieren edge along the metal girder in order to find the position of the focal point of the lens L3. The rate of schlieren interception is adjusted by putting a candle light at the position of the chamber and moving the schlieren edge (the razor blade) in the transverse direction towards the focal point while at the same time watching the image. The image shows the density gradient field arisen from the heat produced by the candle light.
- When the results of the previous steps in the adjustment procedure are satisfactory the continuous light source is replaced by the flash light source. In this step the flash light source one extra lens together with lens L1 are to be adjusted so that the flash light will be focused at the hole aperture HA. The positioning of the flash light source and the two lenses can be simplified by using a small Maglight torch instead of the flash light source. The torch lamp has approximately the same size as the aperture of the flash light source and since it has a continues light the positions of the light source and lenses are easily determined. Only small corrections to these positions are required.
- In the last stage of the adjustment procedure experiments with shock waves are carried out where the light conditions, the light intensity and the rate of schlieren interception are checked. To obtain quick information about the light conditions a Polaroid camera back was used. The light intensity showed to be too large and for this reason two polarization filters were put between the lens L4 and the camera in order to reduce the intensity of the light reaching the image screen. By studying the shock image on the Polaroid photographs the rate of schlieren interception could be verified. In obtaining good light conditions a trial and error procedure was used,

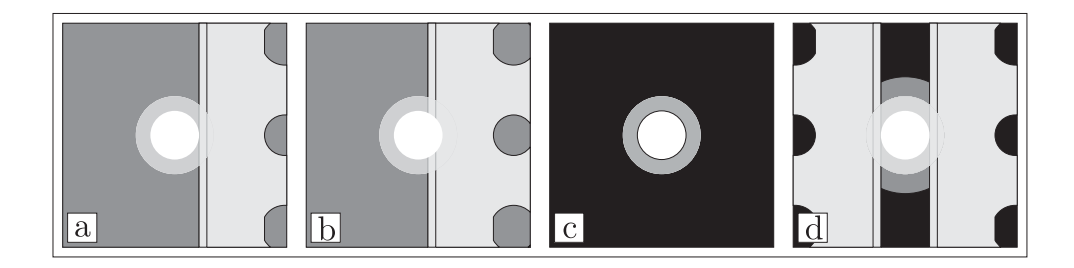


Fig. 19. Schlieren interception methods.

making adjustments, taking a picture and then if necessary making new adjustments.

3.2.4 Light conditions and disturbing light reduction

In section 3.1.2 two different discharge devices used to produce shock waves are described. A discharge gives rise to an unwanted light. A certain amount of this light will take the path through the second schlieren appliance. If no measures are taken to avoid this light from reaching the camera it will disturb the image on the photographic plate. The first device used to produce weak shock waves gives only a small quantity of disturbing light. This disturbing influence can be reduced by correct adjustments of the optics and flash unit, in order to obtain as much light intensity as possible into the parallel light section. If the flash light intensity is 'large' compared to the intensity of the disturbing light the influence from the disturbing light is reduced.

The interception of the deflected light can be done since this light will be focused in the close neighborhood of the focal point of the parallel light. In the experiments with weak shock waves two different light interception methods were used. In the first method a razor blade was placed at the periphery of the focal point of the second schlieren lens, see figure 19(a). This method gives a good sharpness and the image of the shock will appear darker than the surroundings. If the razor blade also cuts a part of the focal point of the parallel light both dark and light regions will appear in the image, see figure 19(b). In the second method a hole aperture was used to intercept the deflected light, see figure 19(c). The hole aperture was made of a thin glass plate covered by a thin layer of black paint except for a small circular area that has approximately the same size as the focal point. This method was used in some attempts but has the disadvantage of giving a less sharp image of the shock wave.

The second discharge device used to produce stronger shocks is much more powerful and gives a much larger quantity of disturbing light than the

first device. Since the light from the discharge is spread rather than parallel, its focal point is spread on a larger area around the focal point of the parallel beam. To cope with this situation several changes in the set-up where made. The first measure was to shield the source, the area in the chamber where the discharge takes place. This was done by painting a circular area at the center of each glass plate black. The radius of these black areas was about $2\,cm$ which is smaller than the radius of the disturbed zone caused by the discharge but is large enough to shield the light from the discharge. The second measure to reduce the disturbing light was to move the chamber further away from the second schlieren appliance in order to reduce the solid angle between the chamber center and the periphery of second schlieren lens. Despite of the measures described above the disturbing light reaching the photographic plate still created some problems.

In order to reduce these disturbances satisfactory the disturbing light is intercepted at the focal point without ruining the principle of the schlieren interception method. This was made by means of two razor blades placed on both sides of the focal point, see figure 19(d). A hole aperture much larger than the original focal point was placed behind the razor blades. This arrangement formed a rectangular shaped shield to the disturbing light as it at the same time will intercept the deflected light originated from the propagating shock wave.

3.3 Time control and measuring

A delay unit was utilized to catch the propagating shock wave at different instants. It turned out that the adjusted time-delay deviated as much as $5 \mu s$ from the true time-delay, which means that the adjusted delay could not be trusted. To obtain a more accurate time interval between the initial released shock and the time for the flash, a photo diode connected to an oscilloscope was used, detecting both the light from the electrical discharge and from the flash unit. This arrangement allowed to determine the time interval with an inaccuracy less than $0.5 \mu s$. This set-up was changed for the experiments with stronger shocks where the single photo diode was replaced by two photo diodes detecting the electrical discharge and the flash respectively. The reason for this new arrangement was to be able to remove and clean the chamber without ruining the adjustments of the photo diode set-up.

A typical attempt from the weak shock experiments recorded by the oscilloscope is shown in figure 20. The upper signal originates from the time-delay, and the lower signal originates from the lights of the electrical discharge and the flash respectively. The oscilloscope is provided with cursors with the options of horizontal or vertical measurements. In the upper right corner of

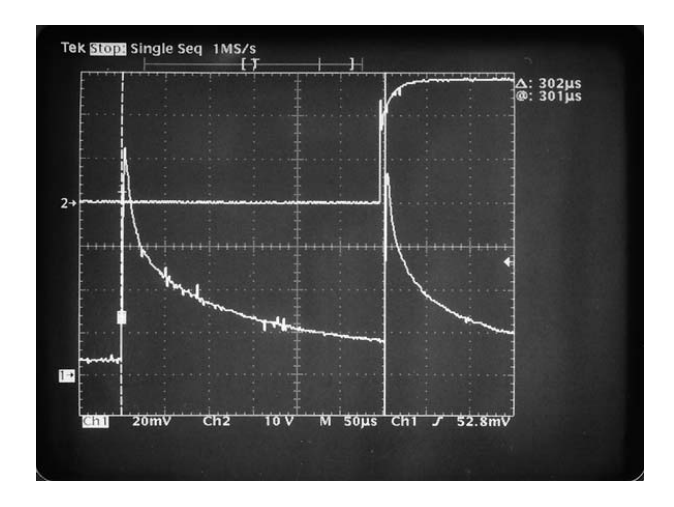


Fig. 20. An oscilloscope record from a typical attempt.

the figure the time-delay between the two pulses of the lower signal is seen. The figure also shows the difference of the adjusted time interval and the measured time interval.

3.4 Shock speed measurements

In the theoretical investigation of the present problem the initial value for the calculations is taken as the Mach number of the circular cylindrical shock at the moment when the shock first touches the reflector boundary. When comparing the experimental results with the calculations it is of interest to compare this initial Mach number and also the Mach number distribution and geometrical shape of the reflected shock.

In order to estimate the shock speed at the moment of reflection in the weak shock case, double exposed photographs were used. The distance Δs between two subsequent shock positions was measured on the photographs and the time Δt between the two photo flashes was registered by a photo diode connected to an oscilloscope. For weak shocks the change in shock speed is small and almost linear so that the shock speed can with good accuracy be estimated as $u \approx \overline{u} = (\Delta s) / (\Delta t)$. This method does not apply to stronger shocks due to the larger and nonlinear changes in the shock speed between two subsequent positions.

3.4.1 The shock speed estimation system

One method to estimate the speed for stronger shock waves is to measure the time instants when the shock passes subsequent radial positions. The

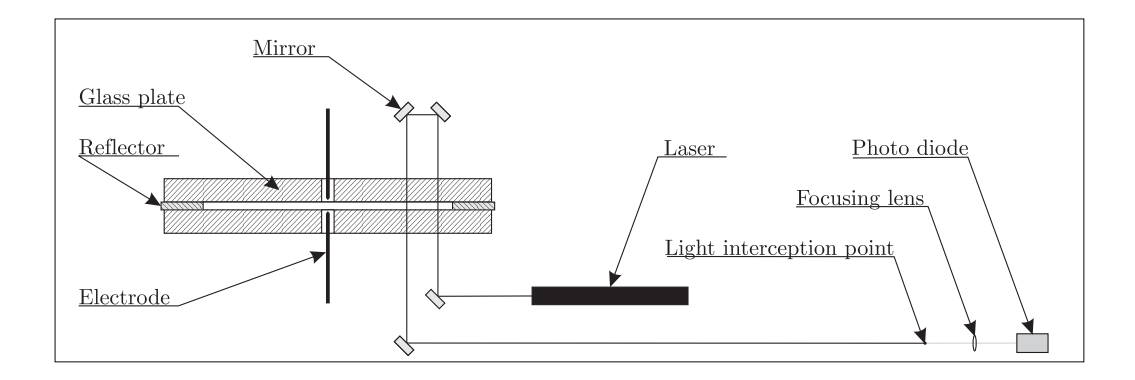


Fig. 21. Shock speed measurements with a laser system.

shock speed is then obtained by taking the derivative of a curve fitted to the measured (t, r) values. For this purpose a time measuring laser system was built.

A laser beam is mirrored twice through the chamber glass plates at two positions located in the radial direction of the chamber and with a distance of about $2\,cm$ apart, see figure 21. The beam continues to an interception point and to a lens that focuses the light on a photo diode. The physical background for this method is the same as for the schlieren method, *i.e* when the shock wave passes the beam the light is deflected. However, the method to register the course of events is different. In the schlieren method the deflected light that originates from the shock wave area is intercepted at the focal point of a schlieren lens. In the present method there are no schlieren lens and the lens that is seen in figure 21 is just there to focus the light on the photo diode. Also, in this method the parallel beam is intercepted while the deflected light, originated from the moment when the shock passes the beam positions, is taking a path beside the interception point.

A picture of the set-up is shown in figure 22. The laser beam is produced by a HeNe laser of power $5\,mW$ that is placed on top of a rectangular aluminum section having the exterior dimensions $b \times h \times l = 250 \times 80 \times 1800\,mm$. At one end of the section a specially shaped plate is mounted and on top of that four holders for mirrors are placed. A mirror holder is fixed to the plate by pulling a screw from beneath of the plate but can also be moved along a track that is milled out of the plate, one track for each mirror holder. The mirror holders are provided with a system of springs and adjustment screws for angular adjustments of the mirrors. The fork shape of the plate is designed to leave a space for the chamber to fit in. In the opposite end of the rectangular section the interception device, the lens and the photo diode are placed. The interception device consists of a thin strip of tin-plate

having approximately the same width as the laser beam diameter which is about $2\,mm$. The section is placed on top of a machine stand provided with a coordinate table which makes it possible to adjust the beam positions to the chamber. In order to relate the beam positions to the chamber boundary two rules that are graded every $0.5\,mm$ are placed on each side of the chamber on the glass plates. The registration of the events when the shock is initiated by the discharge and then passing the beam positions is registered by two photo diodes which are connected to the oscilloscope which records the events. One would argue that the beam diameter is considerably larger than the thickness of the shock wave but since the registration of the events is similar and repeatable for the two beam positions, the pulses recorded by the oscilloscope are expected to be well defined.

The geometry of the reflector boundary can be described to have a symmetry radius at every 36° angle, at the reflector corners and the reflector sides. It is therefore reasonable to assume that if the initial shock is symmetric along the shock front and is centered in the chamber, the reflected shock will be symmetric along these symmetry radiuses. At other locations the shock may propagate along curved paths which are unknown for the experiments. For this reason the measurements can only be performed along the symmetry radiuses. A number of measurements along a symmetry radius gives a number of measured point in time and position (t, r). Since the shock passes the two beam positions twice during the outward propagation and the inward propagation the results from one attempt give a total of four pairs of by the shock traversed positions and times.

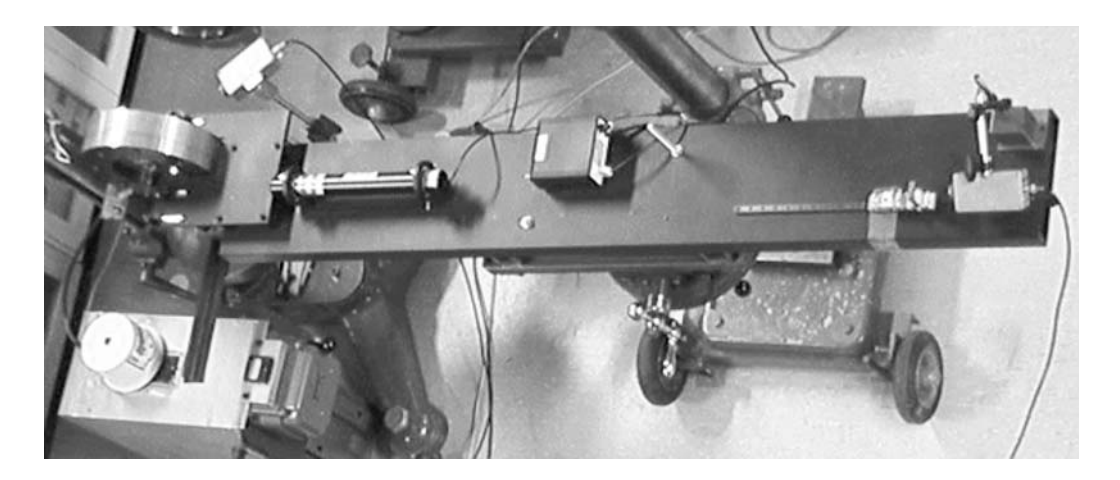


Fig. 22. The laser system setup for shock speed measurements.

3.5 Experimental procedures

3.5.1 Weak shock experimental procedure

Before any experimental attempts were made the performance of the current discharge device, the strength of the obtained shocks, was unknown. This implied that the time it takes for a shock to propagate the distance from the center of the chamber to a desired position in the chamber could not be known in advance. In order to get a decent start of the experiments a typical time-delay was needed, i.e the delayed time from the moment when the shock is initiated until the moment of the flash. To estimate a typical time-delay, an assumption that the shock is propagating in air with a constant Mach number M=1.5 was made. The radius of the reflector boundary is about $R=80 \, mm$ and the speed of sound in air at normal conditions is about $c_0=340 \, m/s$. A typical time-delay was then estimated as $t=R/(Mc_0)\approx 157 \, \mu s$. The assumption of a constant Mach number is not correct, but the simple calculation above turned out to be sufficient for the preceding experiments.

As the results started to emerge, a more and more reliable sense about the light-conditions and the times of propagation, appeared. This sense was based on the procedure of the adjustments done before the attempts and the results from the Polaroid photographs. Since the size of the Polaroid photographs result in a poor resolution when scanning, enlarged copies from ordinary film roles had to be used. In addition, the use of ordinary film instead of Polaroid, allowed a more frequent experimentation. Different types of film roles were tested and the choice fell on a black & white Kodak Tmax ISO 400 film, processed as an ISO 3200 film (+3 steps). The reason for processing the film as an ISO 3200 film was that the light condition adjustments were carried out with a ISO 3000 Polaroid film which was the only available Polaroid film with a larger light sensitivity than ISO 100.

The experimental work, trying to photograph shock fronts at different moments, could begin. The performance of a typical 'weak shock' experiment was carried out according to the following scheme:

- The optical set-up is checked and (if necessary) adjusted, and the camera supplied with a new film role.
- In a special record the date, the time, the number of the current attempt and the desired time-delay is noted. The date and the number of the current attempt is written on a tiny slip made from transparency film, placed on the chamber glass plate to be viewed in the photographs.
- The desired time on the delay unit and the division of time on the oscilloscope are adjusted.

- The voltage in the electrode-gap is adjusted by turning a potentiometer on the electrical discharge device.
- · The laboratory is blacked out.
- The delay unit and the oscilloscope are reset.
- The camera shutter is opened and the discharge device button is pushed. The electrical discharge is released and the delay initiated. At the same moment the oscilloscope-sweep starts, recording the signal from the photo diode that register the two light pulses from the discharge and the delayed flash.
- The camera shutter is closed.
- The laboratory is lighted up and the discharge device is turned off.
- The time interval between the two light pulses obtained on the oscilloscope is noted.
- · The equipment is set ready for the next attempt.

3.5.2 Moderate and strong shock experimental procedure

The experience obtained from the weak shock experiments was a good help when preparing the experiments for stronger shock waves. However, a new problem arose that could not be easily taken care of, the disturbing light from the much more powerful discharge. Several hours were spent in order to find a solution to the problem and a lot of unsuccessful experimental attempts were made. Gradually the light condition was improved and the results started to emerge, see section 3.2.4 for details about the measures taken to improve the light conditions.

At the time for these experiments a new Polaroid film with ISO 400 sensitivity was available at the dealer. This together with a much better set-up of the flash light section made it possible to use the black & white Kodak Tmax ISO 400 film processed as normal.

The performance of a typical experiment with moderately strong shocks was carried out according to the following scheme:

• The optical set-up is checked and (if necessary) adjusted, and the camera supplied with a new film role.

• In a special record the date, the time, the number of the current attempt and the desired time-delay is noted. The number of the current attempt and date is printed on a tiny slip made from transparency film, placed on the chamber glass plate to be viewed in the photographs.

- The electrodes are removed from the chamber and the argon gas tube is turned on in order to fill the chamber with argon.
- The wire is applied to the electrodes and is adjusted to about $12 \, mm$. The length of the wire is measured and noted.
- The gas tube is turned off and the electrodes with the wire are inserted into the chamber.
- The desired time on the delay unit and the division of time on the oscilloscope are adjusted and noted.
- The power for charging the capacitor is turned on and the voltage is adjusted to the desired level by turning a potentiometer on the power supply unit.
- · The laboratory is blacked out.
- The delay unit and the oscilloscope are reset.
- The camera shutter is opened and the trigger button for the electrical discharge device is pressed. This initiates the shock and starts the delay. At the same moment the oscilloscope-sweep starts, recording the signals from the two photo diodes that register the light pulses from the discharge and the delayed flash.
- The camera shutter is closed.
- The laboratory is lighted up and the power supply for the discharge capacitor is turned off.
- The time interval between the two light pulses obtained on the oscilloscope is noted.
- The equipment is set ready for the next attempt. After a few attempts (4-5) the chamber has to be dismounted and cleaned before the next attempt.

3.5.3 Shock speed measurement procedure

In the shock speed experiments the laser system described in section 3.4.1 was used, and the shock waves were generated by means of the discharge equipment that is based on the exploding wire technique.

The performance of the shock speed experiments was carried out according to the following scheme:

- The chamber is removed from its machine stand and dismounted. The reflector is rotated to the desired angular position. The chamber is assembled and placed back on the machine stand.
- The shock speed estimation system is brought to the chamber and the laser beam is adjusted to the desired measurement positions and to the photo diode.
- The chamber is filled with argon and a new wire is placed between the electrodes which are inserted into the chamber center holes.
- The power supply to the discharge device is adjusted and turned on.
- The laser is turned on and the oscilloscope is set ready.
- The trigger button for the electrical discharge device is pressed and the shock is initiated. At the same moment the oscilloscope-sweep starts, recording the signals from the photo diode that register the events when the propagating shock is passing the two beam positions.
- The time instants of the four pulses viewed on the oscilloscope are measured by the cursors and noted.
- The experiment is repeated at least five times for the current beam positions. After that the beam is moved to new positions where a new series of measurements are made.
- When the measurements along a symmetry radius are finished the reflector is rotated to the next angular position and a new sequence of measurements are made.

4 Results and comparison with theory

The experiments in the present investigations were carried out for initial Mach numbers in the interval $1.1 \le M \le 1.7$ which covers the range from weak to moderately strong shock waves. In the present work the definition of the initial Mach number is the Mach number of the circular cylindrical outward propagating shock at the instant when the reflection process is initiated. The notion of the initial Mach number strength or shock strength in the present text related to an experimental case will assume the above definition. However, initially the shock does not necessarily has to be weak even if it is the case when it reaches the reflector boundary, also a weak shock at the beginning of the focusing process will eventually be transformed to a strong shock due to the non linear mechanisms of the shock focusing process. In the present work the weak shock case is the situation where the converging shock will undergo a shock crossing process discussed in section 2 where the discontinuities on a shock front corner move together and cross. In the moderately strong shock case the focusing process is different in that the discontinuities on the shock front diverge as the shock propagates in the inner of the chamber. This difference is the main reason for the subdivision of the present section in the weak and moderately strong shock results.

In section 3.1.2 two different equipment to initiate the electrical discharge are described, the first using the 'igniting spark' and the second 'exploding wire' techniques. The former equipment is sufficient for the generation of weak shock but is not able to produce stronger shocks. The latter equipment however, is much more powerful and can probably even produce initial shocks that are close to strong. There is a problem though that the powerful discharge causes a massive disturbance in a zone around the center of the chamber. This disturbance prevents the shock visualization in the vicinity of the chamber center. Stronger discharges create larger disturbance zones. This is rather unfortunate since one of our goal was to study the focusing process as the strength of the shock increases, which happens as the shock approaches the center of the chamber. One of the possibilities to reduce the size of the disturbance zone without reducing the strength of the discharge is to replace air by another gas. Argon showed to have better qualities in this respect.

Some of the experimental results for the weak shock case have been published earlier in the journal WEAR, Johansson et al. (1999), where also a comparison with a calculation based on acoustic approximation is presented. These results will be repeated below for completeness of the description of the experimental investigation and also the new results will be presented. The results of the stronger shock experiments are new and are a substantial

contribution to the present work.

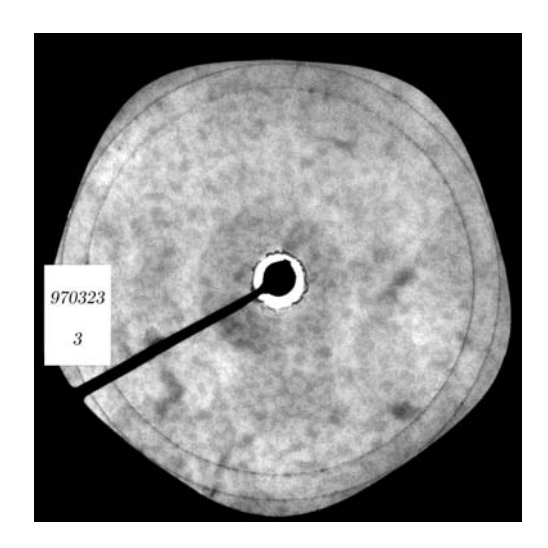
4.1 Shock speed estimation

Before the details of the results from the different shock speed estimations are presented we have to clarify the geometry of the present problem. The reflector boundary geometry used in the present work possesses five lines of symmetry each 72° that goes from a reflector corner to a reflector side. Each symmetry line can be said to consist of two symmetry radiuses, one that begins at the center of the chamber and ends at a reflector corner and the one that begins at the center of the chamber and ends at a reflector side. These radiuses can also be related the angles 0° and 36° which correspond to a reflector corner respectively reflector side. These angles are just two values of the angle φ in equation 1 shown in section 2. If the strength of the initial shock is uniform along the shock front and the shock is symmetrically positioned in the chamber these symmetry radiuses will be the locations where the reflected shock will have its symmetries, at the sides and at the corners of the shock. The rays along which the shock is propagating are at these locations straight lines.

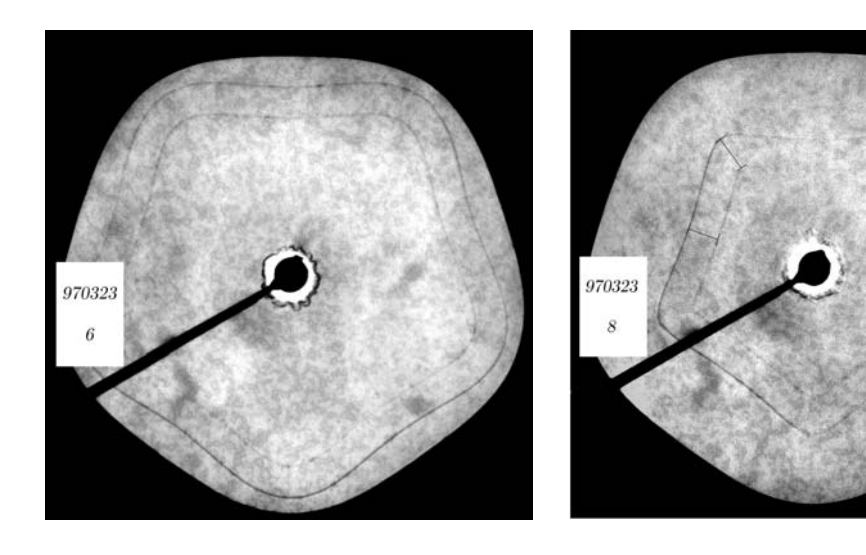
4.1.1 The speed of the weak shocks

In section 3.4 a simple and fairly accurate method to estimate the shock speed of weak shock waves by utilizing double exposed photographs was discussed. Figures 23(a) through 23(c) show three double exposures at three different attempts performed in air, figure 23(a) before and figure 23(b) and 23(c) after reflection. The shock speed is estimated by dividing the radial distance and the time difference between two subsequent positions of a propagating shock front. To determine the radial distance enlarged photographs were used where the reflector diameter value and the radial distance value were measured with a slide calliper and then compared and scaled with the real reflector diameter. The difference in time between two subsequent exposures were measured by an oscilloscope connected to a photo diode that registers the two photo flashes.

The outward propagating shock wave viewed in figure 23(a) has a radial distance of $\Delta s = 8.8 \, mm$ between the two positions and the time between the two exposures is $\Delta t = 23.0 \, \mu s$. Since the change in shock speed of a weak shock can be considered to be close to linear this gives a mean shock speed of $u = 383 \, m/s$. Expressed as a Mach number with the speed of sound in air taken as $c_{air} = 340 \, m/s$ this gives $M = 1.12 \pm 0.03$. The magnitude of this Mach number can also be taken to be valid closer to the reflector boundary,



(a) Cylindrical shock before reflection, $141/164\,\mu s.$



(b) Reflected shock at $196/224\,\mu s.$

(c) Reflected shock at $245/274 \,\mu s$.

Fig. 23. Double exposed photographs.

the 'initial Mach number', this since the change in shock speed along small distances is negligible for a weak shock. The radial distance between the two locations was measured at several angular positions and the results showed a symmetry in shock speed along the front. Several attempts at corresponding shock positions showed a stability in shock speed which implies that the current discharge equipment was stable.

For a shock right after the reflection the local shock speed at the two angular positions 0° and 36° differs from that of a pure acoustic shock. In the present weak shock case due to the relatively low initial Mach number the difference from the acoustic case is almost negligible at least at locations close to the reflector boundary where the curvature at the shock corners are still large. This was confirmed by measurements made along the two symmetry radiuses on the figure 23(b) where no difference in shock speed could be found and the Mach number at these positions was estimated as $M=1.09\pm0.03$. In the figure 23(c) a shock front closer to the chamber center is shown and a difference in shock speed at the two angular positions could here be confirmed. When doing the same measurements as for the previous case the local shock speeds were found to be $u = 364 \, m/s$ at the shock front sides and $u = 414 \, m/s$ at the shock front corners. The corresponding Mach numbers at the shock front sides respectively corners related to the chamber fix system was then found to be $M=1.07\pm0.03$ and $M=1.22\pm0.03$ respectively. The chamber fix system is used since the oncoming flow ahead of the reflected shock is unknown. This flow is necessary to determine a Mach number in reference frame fixed to the flow.

4.1.2 The speed of the moderately strong shocks

In section 3.4.1 a laser system for shock speed estimation at different positions in the chamber was described. A laser beam passes twice through the chamber glass plates at two positions located in the radial direction of the chamber with a distance of about $2 \, cm$ apart, see section 3.4.1 for more details. When the shock passes these positions the beam is deflected and the events are registered by a photo diode connected to an oscilloscope.

The oscilloscope sweep starts when the shock generating discharge is released and continues during a time in which the shock passes the two beam positions twice, first on the way outwards before reflection and then on the way inwards after reflection, see figure 24 where the two beam positions are passed by the initial and the reflected shock fronts. An oscilloscope picture from a typical attempt is viewed in figure 25 where four pulses separated in time are shown. The first two pulses arise when the outward propagating shock passes the two beam positions and the next two pulses arise when the

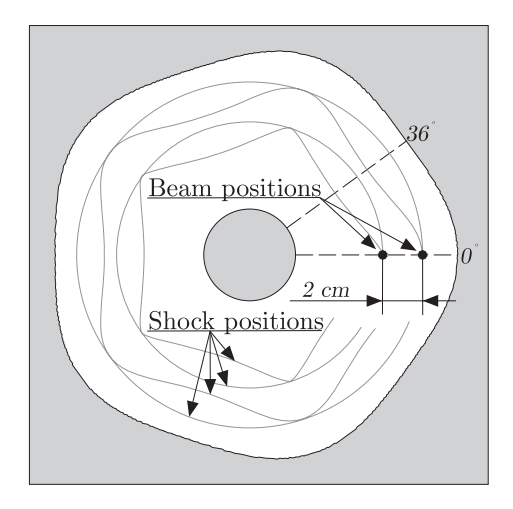


Fig. 24. Laser beam positioning.

reflected shock passes the same positions in the opposite order. The time value for a pulse was measured both at the pulse front edge and at the pulse top value. The top value measurements showed to give more reliable results. As a result from an attempt the four pulses together with the beam positions give a total of four pairs of the shock positions and times, (s,t).

One would wish to be able to measure the shock speed at all locations in the chamber but the chosen method does only admit measurements along the symmetry radiuses where the shock front is symmetric and is propagating along well defined rays which are straight lines. The shock speed measurements were performed at three different shock strengths corresponding to the discharges at three different voltage levels $(1.8 \, kV, \, 2.4 \, kV \, \text{and} \, 3.0 \, kV)$. For each shock strength the shock speed measurements where carried out along the two symmetry radiuses at the angular positions 0° and 36°. Unfortunately the measurements could not cover the hole radial range of the chamber, this since the presence of the discharge gives rise to a disturbed zone around the chamber center that prevents the signal to be viewed on the oscilloscope. The interval which could be covered was the distance between the radius $30 \, mm$ and the reflector radius at the current symmetry radius. In this interval measurements where made at intervals of 5 mm and at an interval of 2.5 mm at positions near the boundary. At least five attempts on each position where made, this to obtain a statistical basis for estimation of the measurement accuracy.

The results of the shock speed measurements for the three different discharge voltages are presented in figures 26 through 29. Figure 26 respective figure 27 shows the shock position at different time instants measured along



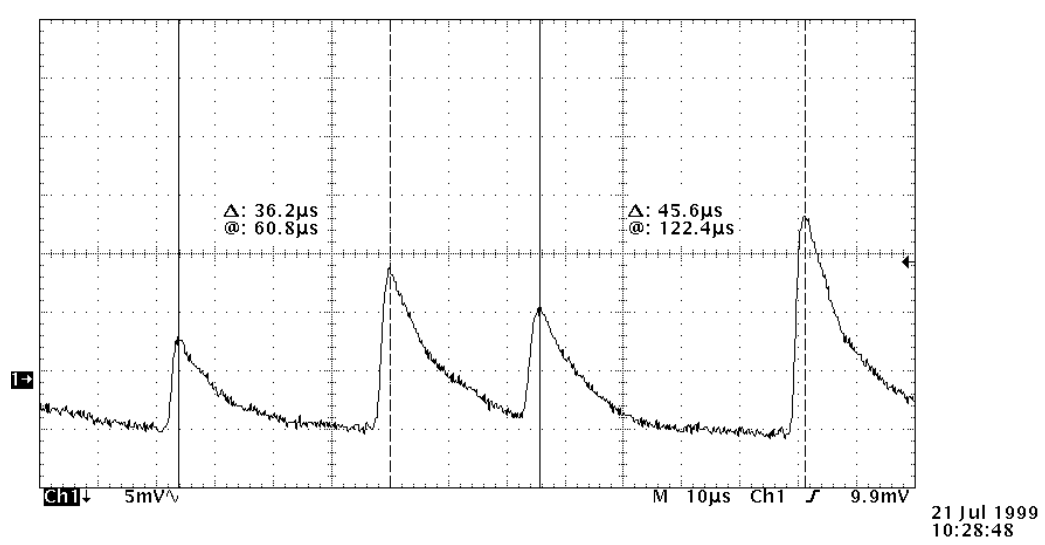


Fig. 25. An oscilloscope picture from shock speed measurements.

the symmetry radiuses at 0° and 36° respectively. The figures show both the outward and inward propagation and each measured time instant is an average of at least five measured values from different attempts. The plot symbols $+, \times$ and * correspond to the different discharge voltages 3.0~kV, 2.4~kV and 1.8~kV. The solid lines are functions fitted to the measured points by means of the least square method. The function used for the outward propagation is

$$t = c_1 r^k + c_2 r + c_3, (14)$$

where c_i are the fitting constants and k is a constant that have to estimated for the specific case. In all considered cases $1.5 \le k \le 1.7$. There is no physical reason for this choice of function, it is only a function that gives a reasonable fit to the measured points. The inward propagation is treated similarly but in this case a r(t) function instead of a t(r) function is used,

$$r = c_1 t^k + c_2 t + c_3. (15)$$

The constant k in this function is chosen in the interval $1.8 \le k \le 2.2$ depending on the initial Mach number and the current symmetry radius. Two additional conditions to this curve fit are the time and the Mach number of the outward propagation when the shock reaches the boundary. The boundary Mach number is obtained by taking the derivative of the outward propagation function at the position of the boundary and dividing it by the speed of sound that in the present case is the speed of sound for argon, at

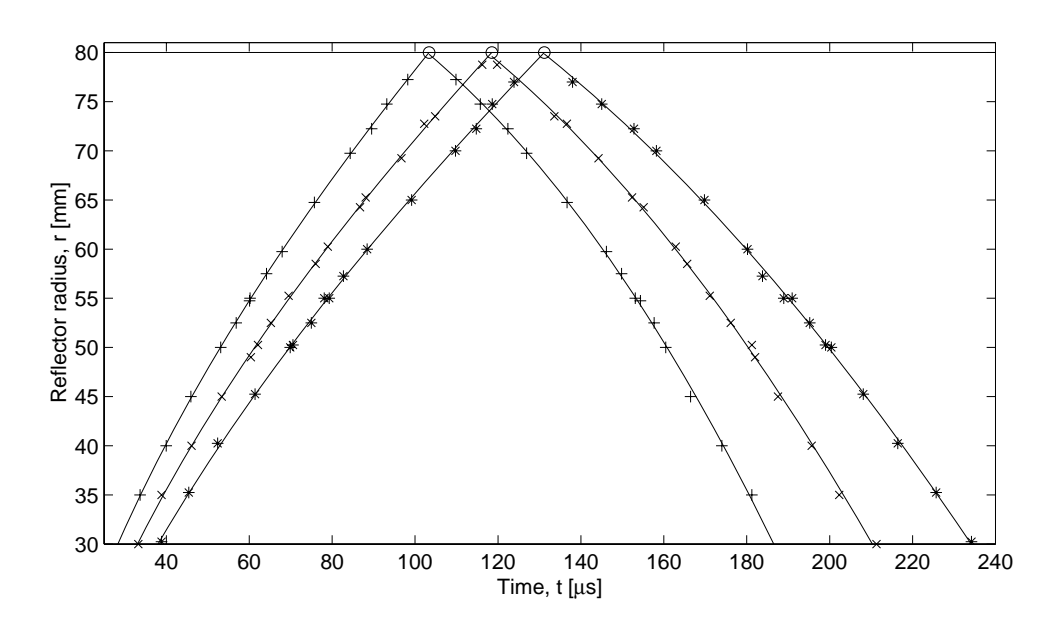


Fig. 26. Shock propagation at the angular position 0° .

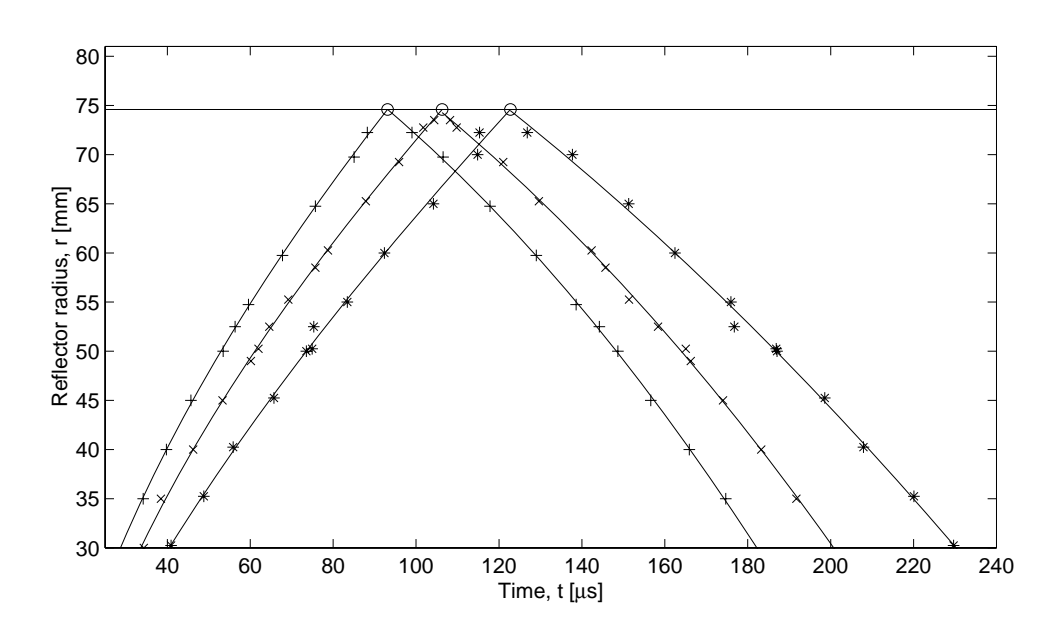


Fig. 27. Shock propagation at the angular position 36° .

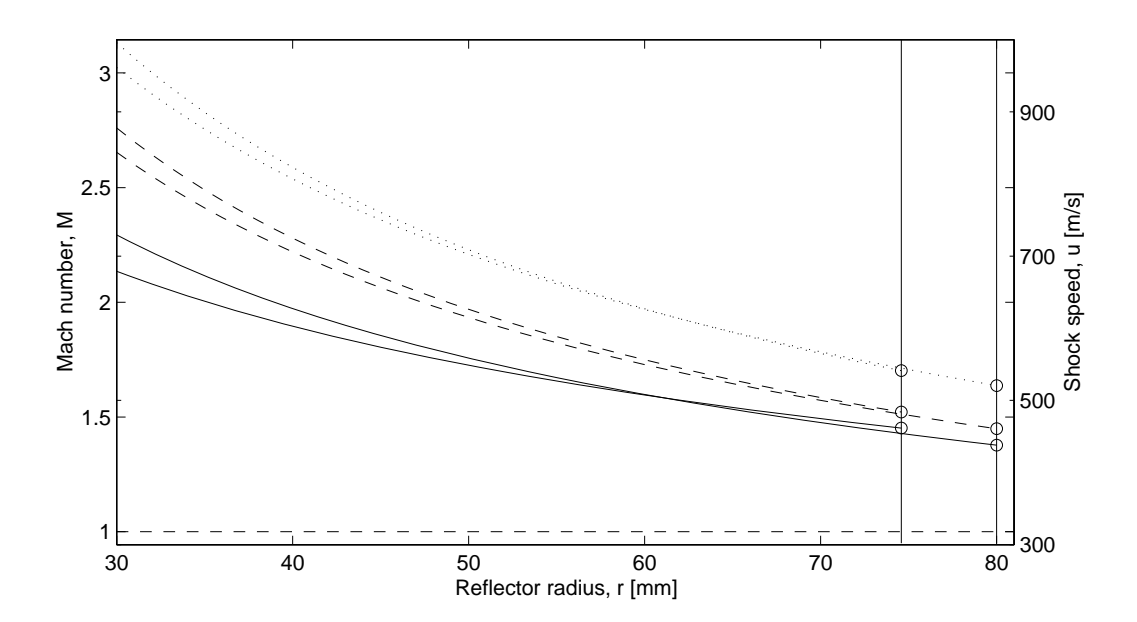


Fig. 28. The outgoing shock Mach number.

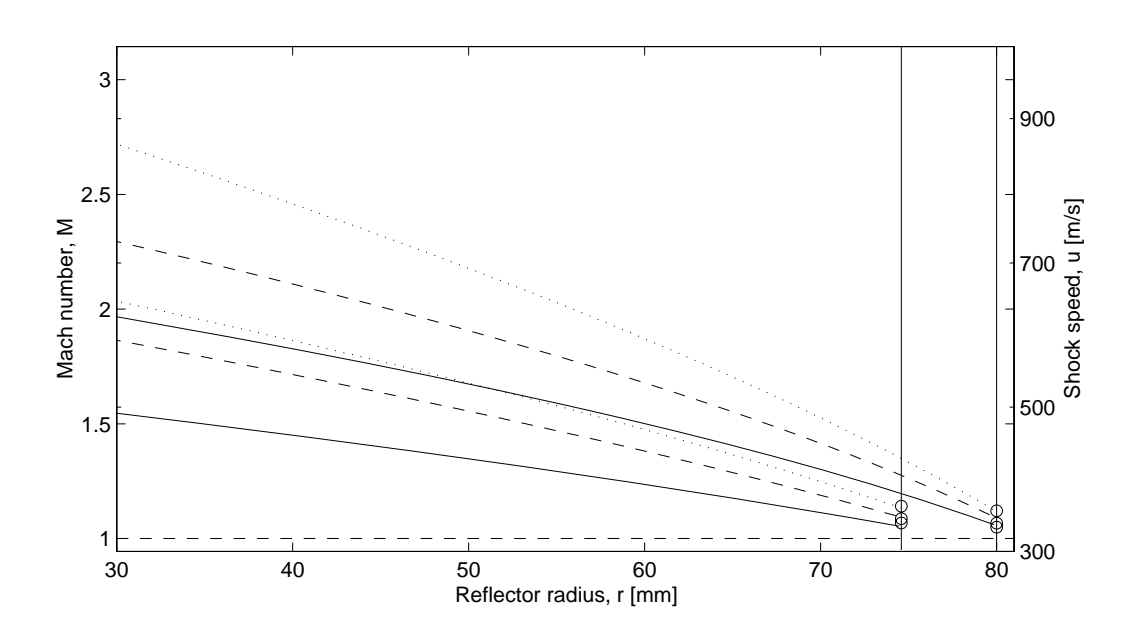


Fig. 29. The converging shock Mach number.

$Voltage \ [kV]$	Angle	M_{out}	M_{in}
1.8	0	1.38	1.05
	36	1.45	1.07
2.4	0	1.45	1.07
	36	1.52	1.09
3.0	0	1.64	1.12
	36	1.70	1.14

Tab. 1. Estimated Mach numbers at the boundary for different discharge levels and angular positions

room temperature equal to $318 \, m/s$. From the normal shock reflection relations the speed of sound and the Mach number of the reflected shock are obtained. These are then used to derive the initial speed of the reflected shock in a system fix to the chamber.

$$u_{r,cf} = M_2 a_2 - u_2 \tag{16}$$

The slopes of outward propagation functions at the positions at 0° and 36° for corresponding discharge levels are almost identical. This is reasonable since the outward propagating shock is supposed to be symmetric for all angles. However, the slopes of the inward propagation functions are not identical. It turns out that the slopes of the functions and consequently the Mach number at the angle 0° are larger than the corresponding slopes or Mach number at the angle 36°. These results are more evident in the figures 28 and 29 where the Mach number and the shock speed at different positions are shown. Figure 28 shows the outward propagation and figure 29 the inward propagation. The curves are obtained by simply taking the derivative u = dr/dt of the corresponding t(r) or r(t) functions and then the Mach number is obtained by dividing the shock speed with the speed of sound. All values are related to the chamber fix system this since the flow conditions in front of the reflected shock is unknown. The estimated Mach numbers at the boundary for different discharge levels and angular positions are tabulated in table 1.

This method where a laser beam is deflected by a passing shock front proved to be a reliable and accurate method to obtain a picture of the speed

Standard deviation interval [%]	$0 < \sigma \le 2$	$2 < \sigma \le 4$	$4 < \sigma \le 5$	total
Number of points	144	18	2	164
Points [%]	87.8	11.0	1.2	100

Tab. 2. Standard deviations of time measurements, 164 (t, r) points.

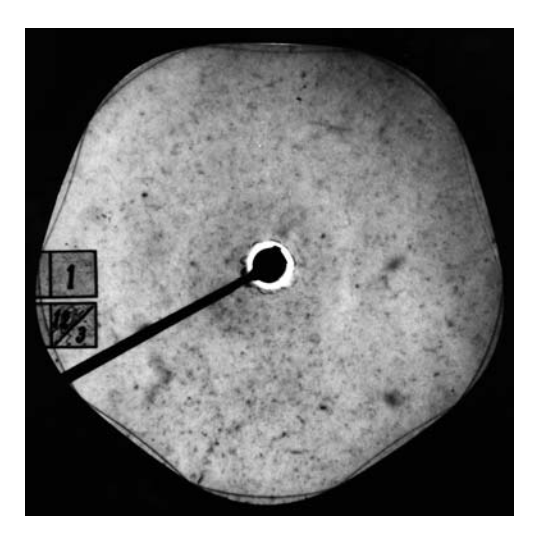


Fig. 30. Shock reflection at the boundary. Time-delay 175 μs .

of the propagating shocks with different discharge strengths and positions of symmetry. In table 2 a summary of the spreading of the time standard deviations for all different measured positions is shown. The standard deviation is here expressed in percent of the mean value time samples at each measured position. As shown the most measured positions have a standard deviation less than 2% and those which are larger than 4% correspond to measurements in which the time interval is short compared to the oscilloscope resolution *i.e.* at positions close to the chamber center.

4.2 The converging shocks

4.2.1 The weak shock propagation

Since the photographic equipment did not allow more than two exposures at each attempt, the only way to catch the shock at different instants was to take single exposures at different times and shock positions, (this does not include the double exposures for the shock speed estimation). However, the repeatability was shown to be good in the sense that the overall picture of the convergence process was the same at various attempts.

Shortly after the electrical discharge is initiated, a circular cylindrical shock wave is formed and starts to propagate outwards in the radial direction with its circular shape preserved. At this stage the medium ahead of the shock is quiescent. When the shock reaches the boundary surface a reflection process starts, see section 2 for theory. The reflected shock front now propagates in the flow created by the circular outward traveling shock.

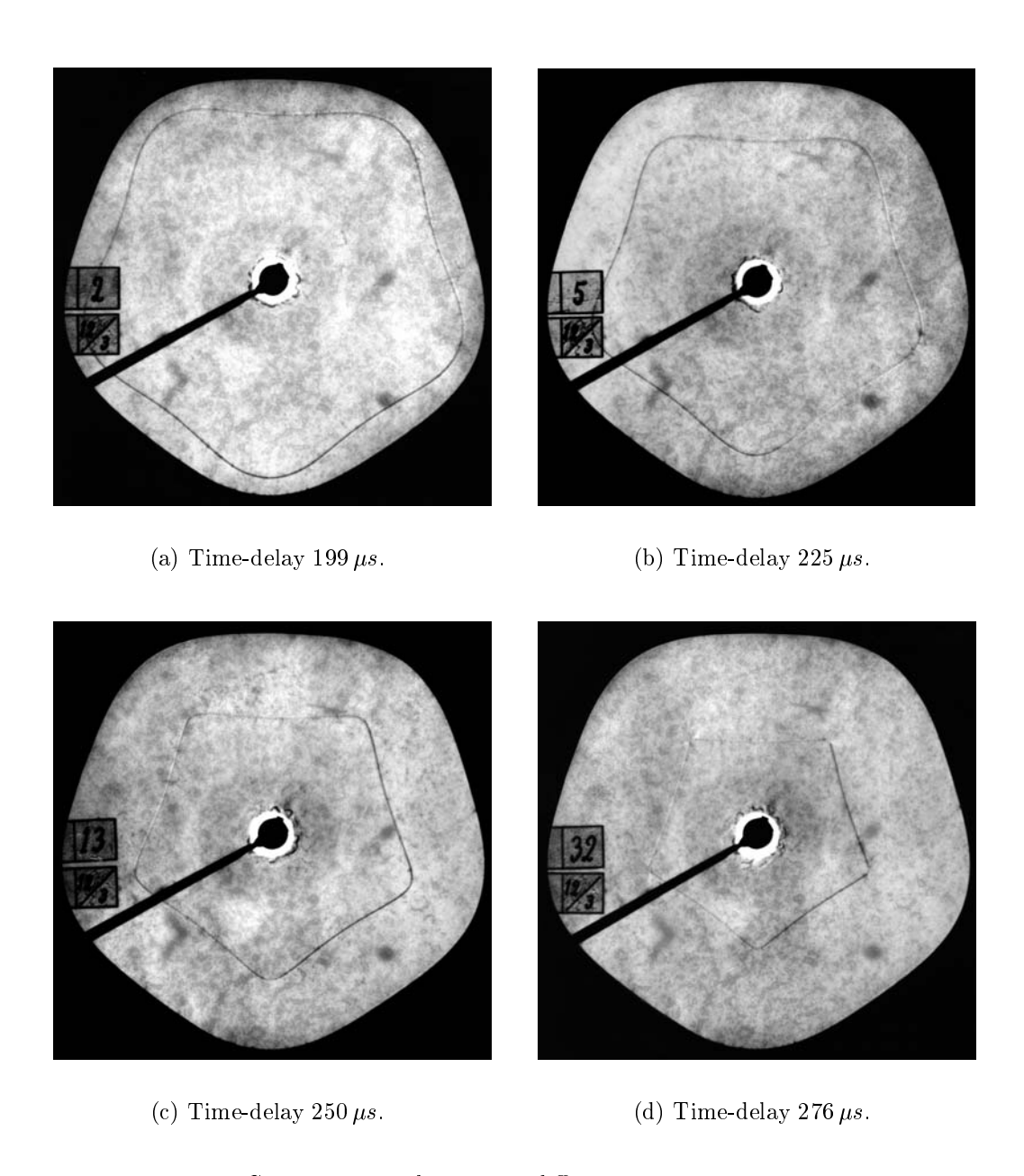


Fig. 31. Converging shock waves at different time-delays, $M_0 \approx 1.1$.

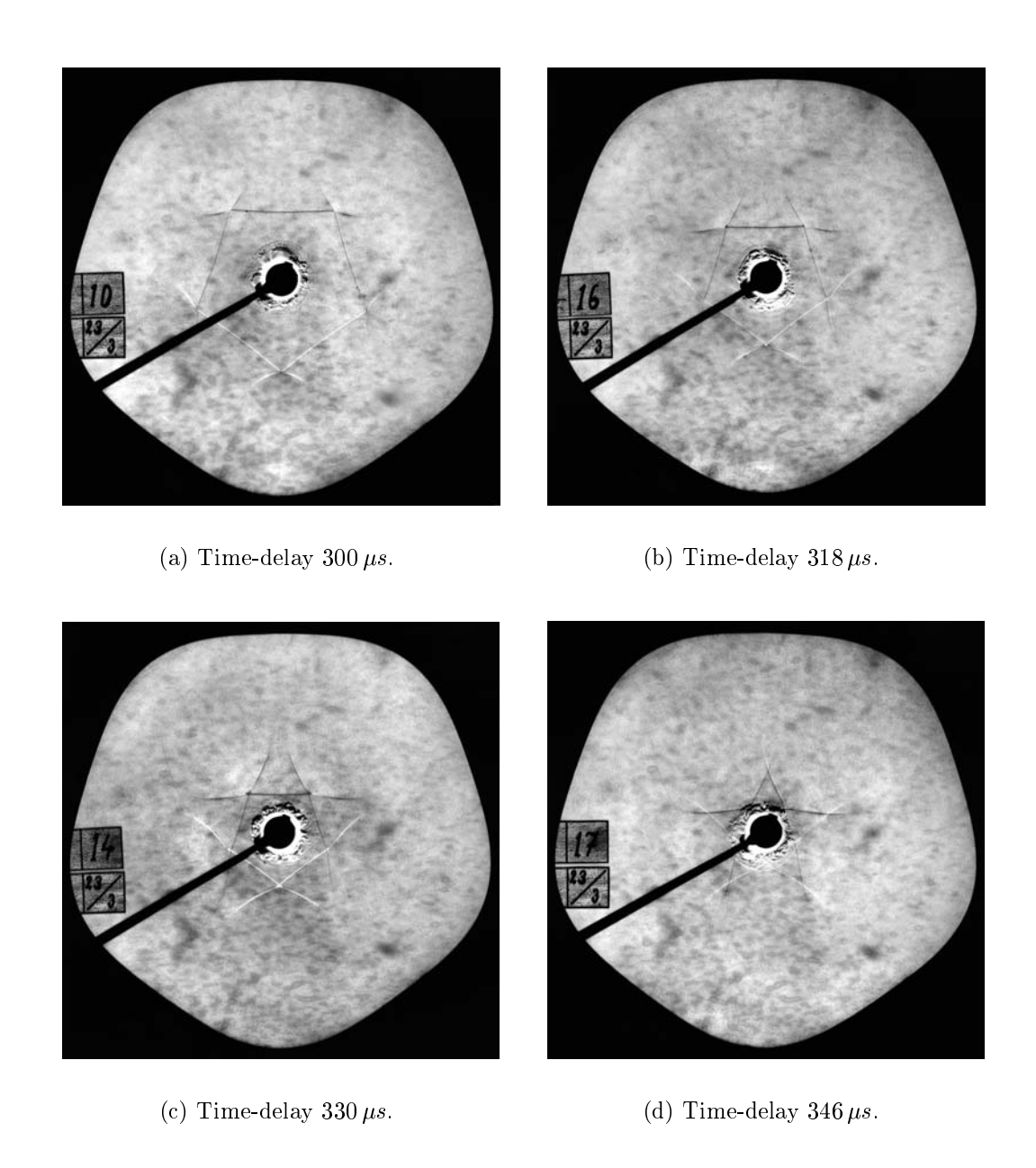
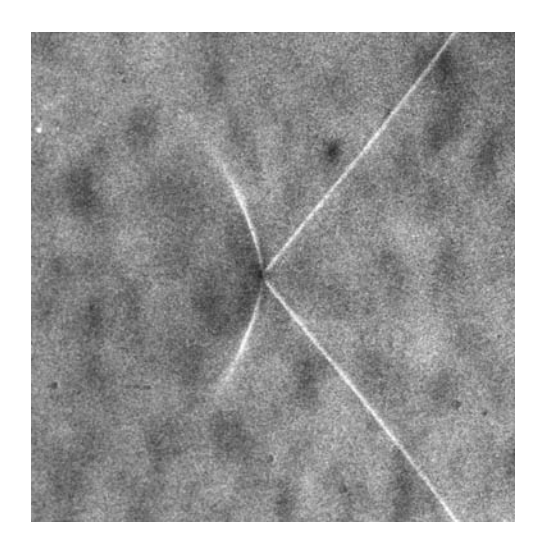
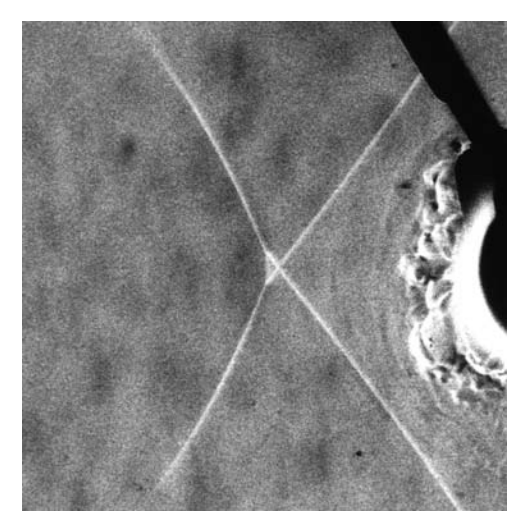


Fig. 32. Converging shock waves at different time-delays, $M_0 \approx 1.1$.





- (a) Shock corner close-up at 300 μs .
- (b) Shock corner close-up at 330 μs .

Fig. 33. Shock waves in focusing process

Figure 30 shows a shock reflection at $175\,\mu s$, where some parts of the shock front are still traveling outwards while some are already reflected. The parts that are still traveling outwards are those, located at the 'corners' of the reflector boundary. These parts of the shock still have the circular shape. At the 'long sides' the reflected parts are seen. When the reflection is completed the whole shock front starts to converge inwards.

During the initial stage of the converging process, each shock front corner becomes sharper while approaching a local focus. This is shown in figures 31(a) through 31(c). However, a complete focusing of the corners into real sharp corners does not occur at this stage. When the shock approaches such a focus the local curvature of the shock front grows and leads to an increase of the local shock strength. The shock is no longer weak at these locations. At a point where the local shock reaches a maximum of curvature where discontinuities in the shock form appear, the so called shock-shocks are formed. In figure 31(d) the shock front has just passed such a point.

Additional feature appears in the picture, that seems to be formations of new shocks behind the corners. This is more evident in figure 32(a). The explanation for this is that the stronger parts of the shock front start to travel faster than the weaker parts and the corners flatten out. This process ends up in a formation of shock-shocks. In the trace of the shock-shocks due to a complex wave field behind, diffracted shocks are formed. This is not an instant event but a gradual process. It can also be described as two

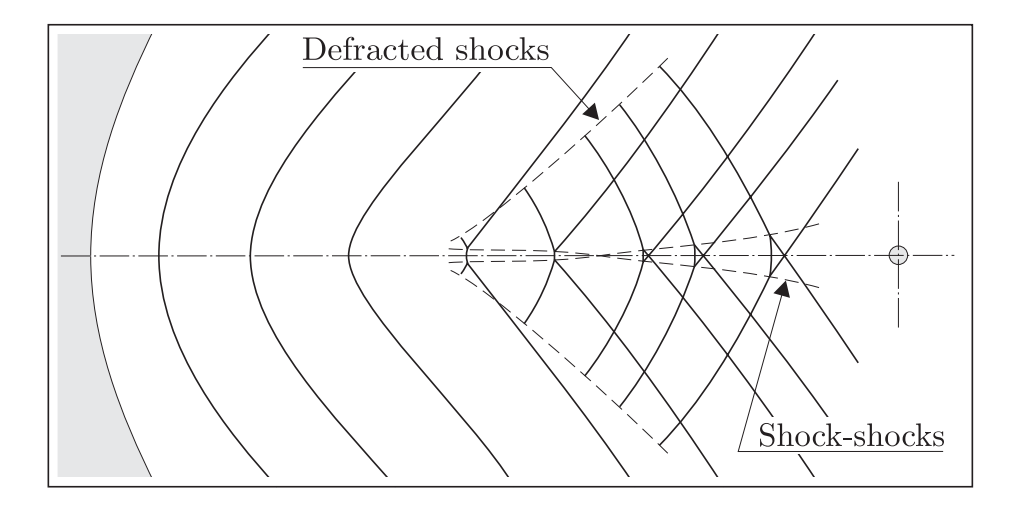


Fig. 34. A schematic representation of the focusing process.

three shock intersections with a common stem shock that are formed in each corner; see figure 33(a) for a close-up of a typical corner of the shock shown in figure 32(a). This corresponds to Mach reflections from each side of a surface located at a symmetry line of the chamber. After this the two shock-shocks at a corner approach each other while the stem shock gets shorter, and a pentagon with sharp corners is formed.

Further development of the focusing process is shown in figures 32(b) through 32(d). The sides of the shock overlap in the corners and form into triangular shaped fronts; see figure 33(b) for a close-up of a typical corner of the shock shown in figure 32(c). The sides in the triangular shapes are called caustics. Finally the shock front converges into the center of the chamber.

A schematic representation of the focusing process described above is shown in figure 34. Here the reflector boundary is located to the left and the chamber center to the right. The shock positions at the different time instants from figures 31 and 32 are shown. While the shock front propagates to the right, shock-shocks arise and in the complex structured flow behind, diffracted shocks are formed. The shock-shocks cross each other and the triangular shape of the caustics appears. This result is in accordance with the acoustic calculation shown in figure 6 in section 2.4.1, except that the acoustic theory does not account for the non-linear conditions that cause the two discontinuities and the resulting stem shock in each corner to appear. If the original shock front is strong this crossing of shock-shocks does not occur: compare the experimental results in section 4.2.2 and the non-linear calculations of Apazidis & Lesser (1996) shown in figure 8 and 9 in section 2.4.2.

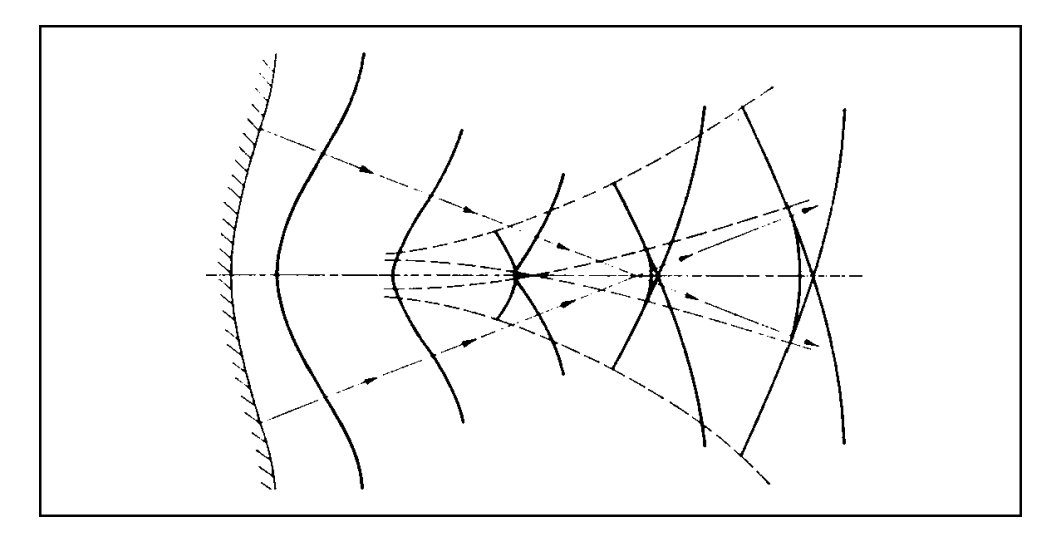


Fig. 35. A plane weak shock wave reflected off a parabolic reflector, from Sturtevant & Kulkarny (1976).

The present case describes the focusing process of a circular weak shock wave reflected off an almost parabolic boundary of comparatively large curvature. Figure 35, from Sturtevant & Kulkarny (1976), describes the focusing process of a weak plane shock wave reflected off a parabolic reflector of small curvature. The similarity between the present case and the case of Sturtevant & Kulkarny is striking, however not at all surprising. The underlying physical mechanism is the same in both cases. A comparison with the experimental results of Sturtevant & Kulkarny (1976) concerning focusing of weak shock waves in a parabolic reflector, can also be of interest.

4.2.2 The moderately strong shock propagation

The initial stage of the moderately strong shock propagation shows features similar to that of the weak shock case. A circular cylindrical shock wave propagates outwards in the radial direction of the chamber cavity until it reaches the reflector where it starts to reflect off the boundary surface. There are some differences though that later on will have consequences for the focusing process during which the reflected shock converges into the center of the chamber. According to the shock reflection relation the reflection angle will become smaller for larger Mach numbers of the incident shock front which entails that the sides of the reflected shock initially will become straighter for larger initial Mach numbers. A larger Mach number of the outward propagating shock will induce a stronger flow field behind the shock front which will have a larger effect on the inward propagation than it will have

for a lower Mach number. According to the calculations shown in Apazidis & Lesser (1996) this flow has a large influence on the shock propagation. These two relations will influence the shape of the reflected shock, the Mach number distribution along the shock front and consequently the continuing propagation and focusing process.

The moderately strong shock experiments were performed at an initial Mach number of $M \approx 1.35$ and the shock was created by an electrical discharge at the center of the chamber using the exploding wire technique described in section 3.1.2. At each experimental attempt single exposed photographs was used and in order to map the course of events at different positions and times. Several attempts had to be made and required a stability in the initial Mach number. This was not a problem since the discharge equipment showed to be very reliable in producing a stable shock strength.

The results for the moderate shock case are presented in the figures 36 through 37 and show the shock from a moment shortly after reflection till the moment when the shock reaches the disturbed flow field around the chamber center. At this discharge level the disturbance is occupying a circular area with radius of about 35% of the chamber radius and this reduces the ability to investigate the focusing process in the vicinity of the center. The beginning of the propagation shown in the figures 36(a) and 36(b) looks familiar to the results from the weak shock experiments, but a comparison of the present shock form with the results of the figures 31(a) and 31(b) shows that the sides in the present case are much straighter. This shows that a larger initial Mach number gives a smaller reflection angle. A comparison of the shock corners in figure 36(c) with those in figure 31(c) shows that the curvature of the corners for the stronger shock is much larger and this is due to the non linear conditions that causes curved parts of the shock to propagate faster than the straighter parts of the shock front. The non linear behaviour of the shock is more evident at the later moments of the focusing process shown in the figures 36(d) through 37(d). In the figure 36(d) we can see that the shock front corners are beginning to flatten out and in the next figure 37(a) this process has led to a creation of discontinuities on the shock front the so called shock-shocks. In the trace of the shock-shocks due to a complex wave field behind, diffracted shocks are formed. The figures 37(b) through 37(d) show the same process as in figure 37(a) but what is not so obvious is that the 'new' sides of the shock front are growing during the propagation while the 'old' sides are shortened. To show this we refer to a closeup, figure 38, of the shock shown in figure 37(d). Except for the shock front, the diffracted shocks and the disturbance in the middle of the picture something new appears in the picture that is known to be the trace of the discontinuities the shock-shocks. The distance between these traces at a 'corner' are seen to grow which

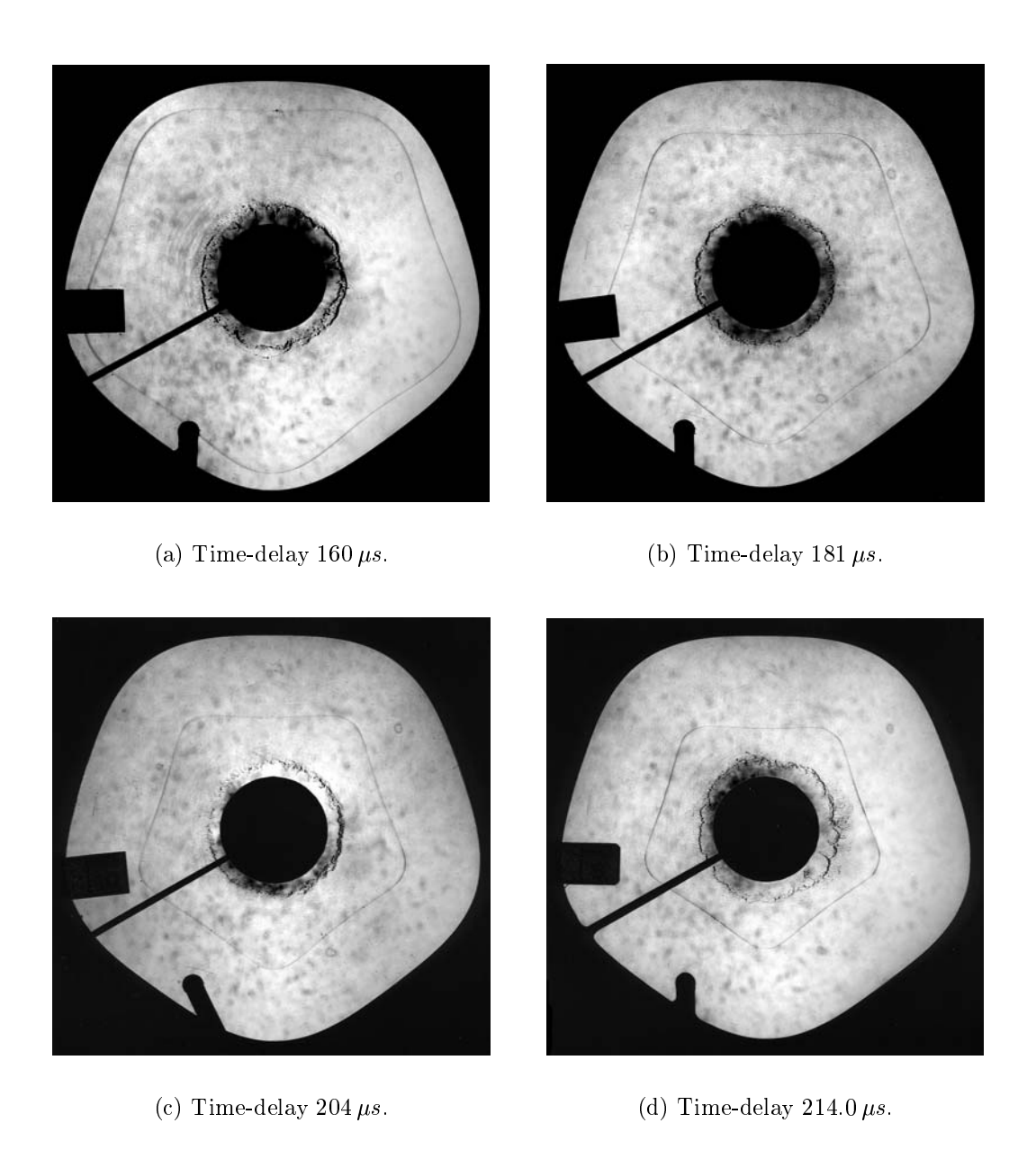


Fig. 36. Converging shock waves at different time-delays, $M_0 \approx 1.35$.

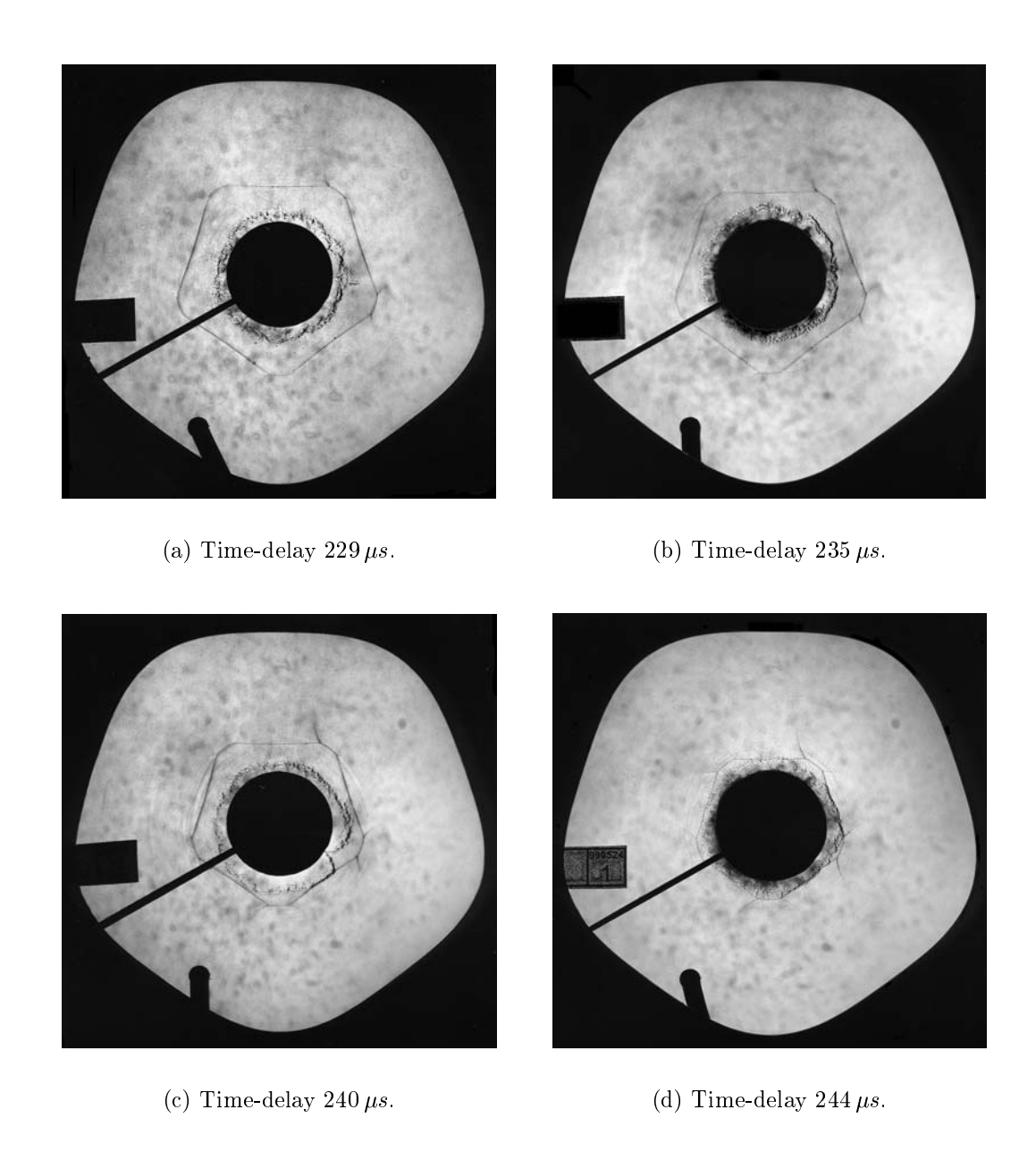


Fig. 37. Converging shock waves at different time-delays, $M_0 \approx 1.35$.

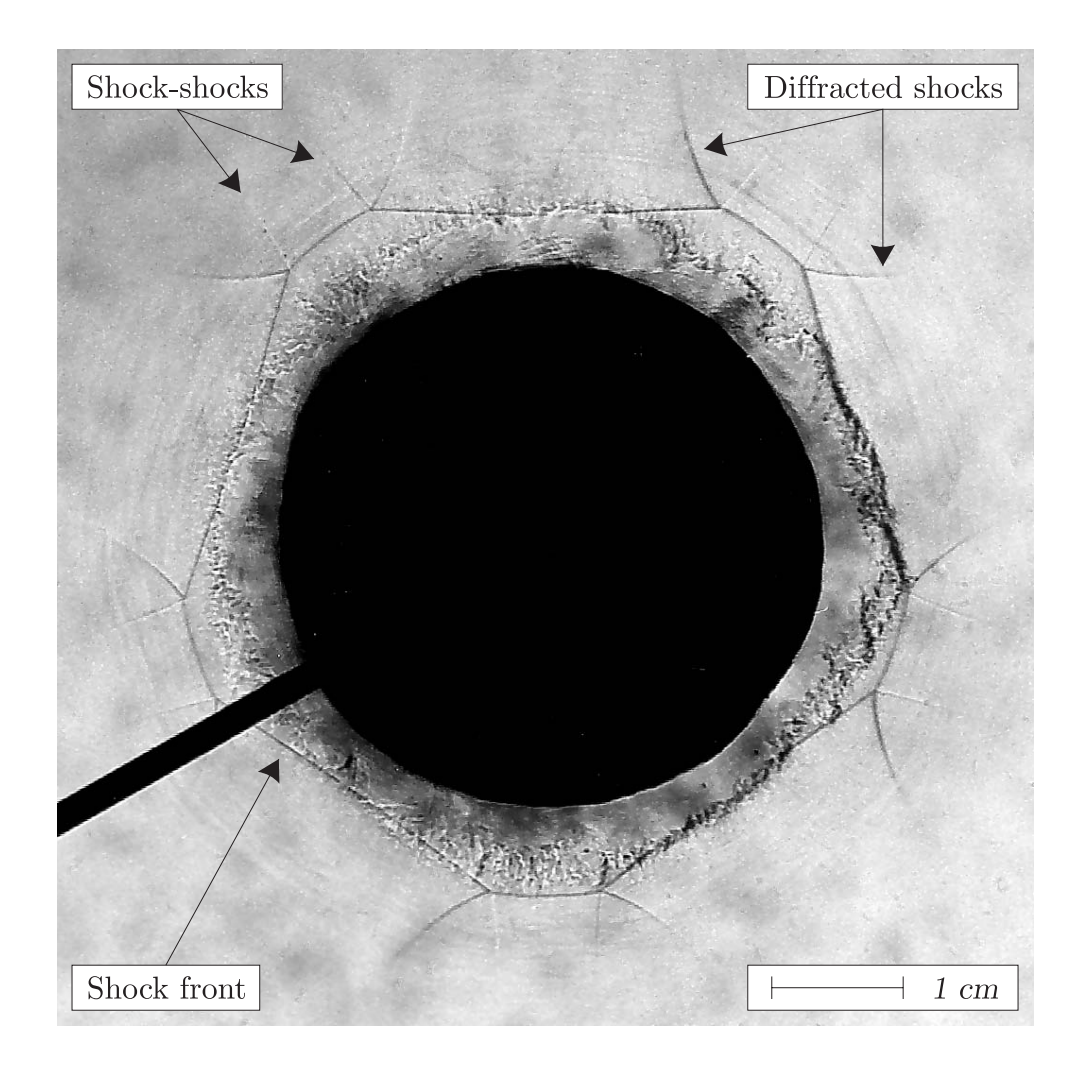


Fig. 38. A close-up at $244 \,\mu s$, shock-shocks and diffracted shocks.

means that the discontinuities moves apart and the new sides do indeed grow in length. The angle between the traces was measured to about 10° which can be used to verify calculations performed at the same initial Mach number. If we could follow the shock propagating into the chamber center we would hopefully experience the rotational behavior of the shock predicted by theory with a pentagon shape with its corner pointing towards the reflector sides.

In the next figures 39 and 40 the results from attempts performed at a larger initial Mach number $M_0 \approx 1.5$ are given. There are no major news in these results compared to the previous case shown in the figures 36 and 37. Some details of the comparison are however of interest. The sides of the shocks in the present case seem to be somewhat straighter than the shock sides in the previous case which once again shows the non-linear mechanism

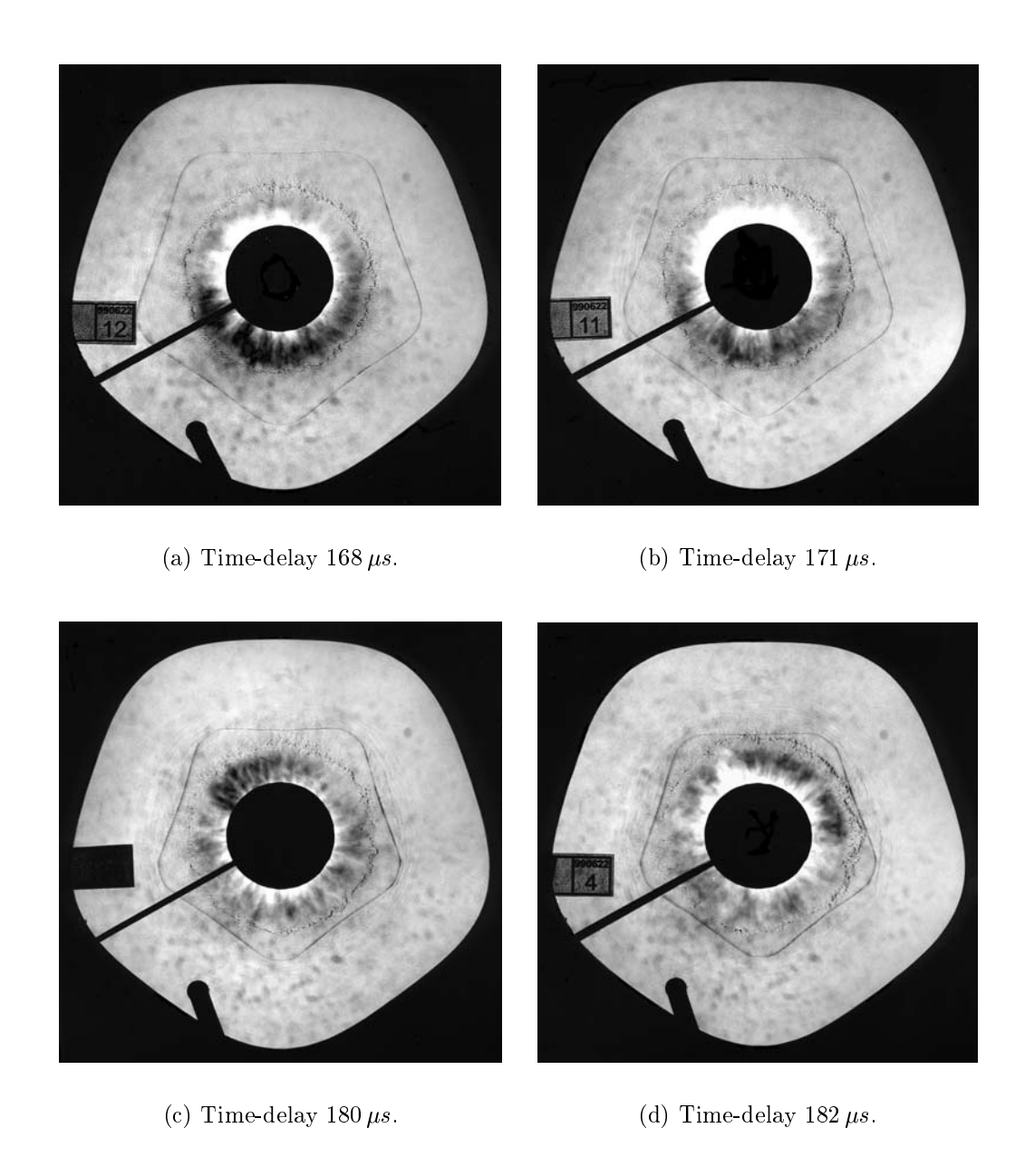


Fig. 39. Converging shock waves at different time-delays, $M_0 \approx 1.5$.

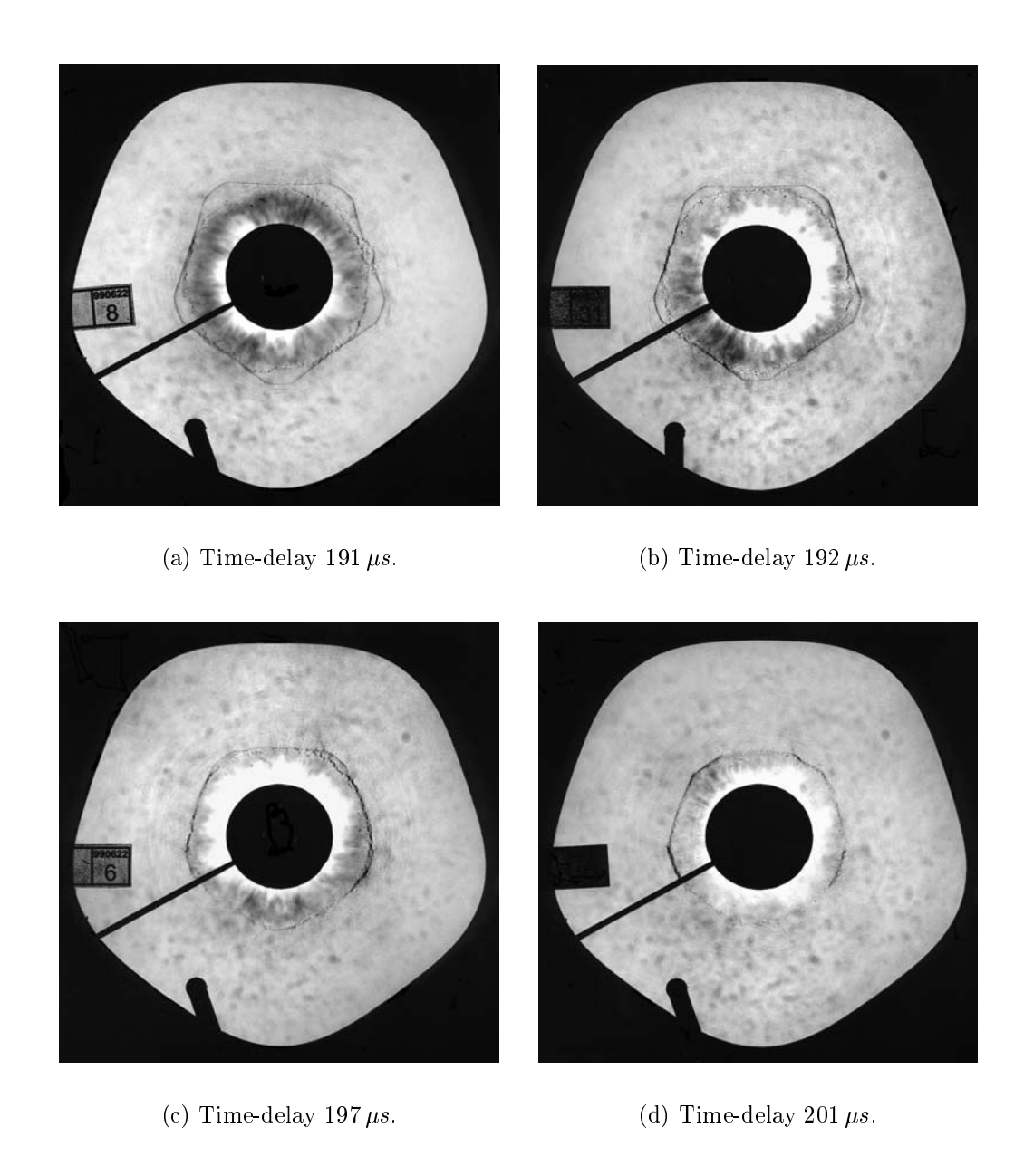


Fig. 40. Converging shock waves at different time-delays, $M_0 \approx 1.5$.

of the reflection and convergence process for higher values of the Mach number. In the figure 39(b) the shock is in the beginning of the phase where the corners of the front are about to become plane. The flattening of the shock front corners seems to appear at about the same radial position as in the previous case but from the results in the present work we can not be certain that this is the case. Comparing the length of the new sides on the shock these seems to be a little bit longer in the present case which confirms the calculated results based on geometrical shock dynamics performed by Apazidis. The longer sides of a shock having a larger initial Mach number implies that the rotational behavior described in section 2 will appear at a larger radius than for a shock having a smaller initial Mach number. This can unfortunately not be confirmed in the present investigation this since the area of interest where the rotation takes place is occupied by the disturbed flow field created by the discharge. In the last figure 40(d) the shock are seen to propagate into the disturbed area in the center of the chamber.

The radius of the disturbance is at the present conditions about 50%of the chamber radius which is a further limitation of the area of interest. If we raise the discharge voltage in order to obtain a larger initial Mach number the area of interest will be further reduced and consequently this method to produce the shock has its limits. Results from attempts at larger Mach numbers confirm the discussion above and the main reason for not showing these results is that the focusing areas are partially covered by the disturbance. In order to be able to catch the focusing process for a strong shock a new and better method to produce the initial shock with a less disturbance has to be invented which is not a trivial task. A possibility to overcome this obstacle would perhaps be to manufacture a new chamber of a larger size. As seen in section 4.1.2 the speed of the outward propagating shock decreases with the radius so this idea is perhaps not the right way to continue. Another possibility might be to chose a different geometry of the chamber where the shock is initiated at one point in the chamber and where the reflected shock is converging towards another point a distance away from the first point.

Once again we make a comparison of the present configuration with that described in Sturtevant & Kulkarny (1976) where an initially plane shock is reflected off a parabolic reflector of small curvature, see figure 41 from Sturtevant & Kulkarny (1976). In this figure the converging shock is assumed to be strong but how can we then compare this situation with the present situation where the initial shock is a moderately strong shock? This is the borderline case but since the shock during the propagation will increase in shock strength this comparison is correct to make. The similarity between the present case and the case of Sturtevant & Kulkarny is also in this comparison

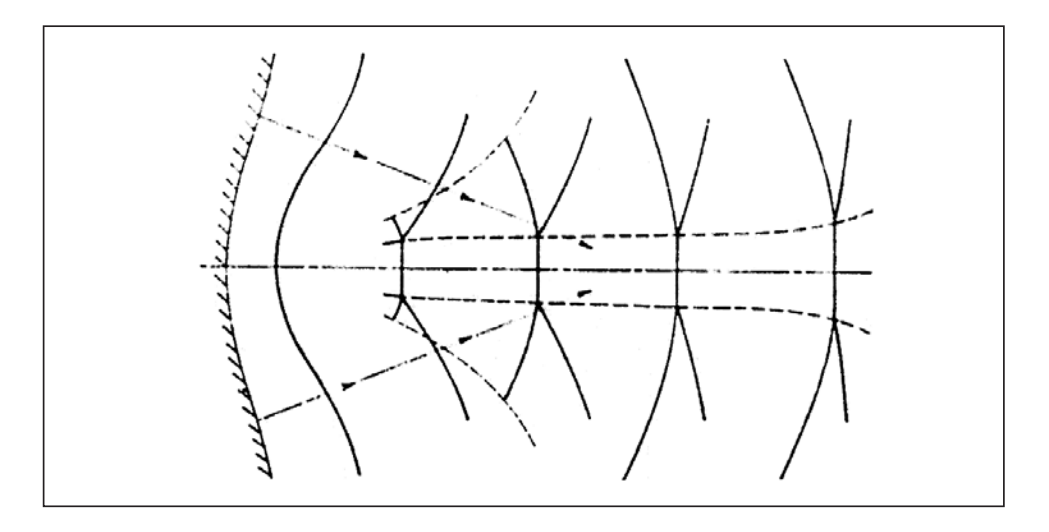


Fig. 41. A plane strong shock wave reflected off a parabolic reflector, from Sturtevant & Kulkarny (1976).

striking, since the underlying physical mechanism is the same in both cases.

4.3 Comparison with some theoretical results

One of the important features of the present work is to compare calculated results with the experimental results shown above. A comparison of the shock form as well as the shock speed will be shown in the present section. We start with the weak shock experiments and compare the shape of the shock at different locations in the chamber with two different calculations, the first is based on geometrical acoustics and the second is a calculation with initial Mach number $M_0 = 1.1$ and is based on geometrical shock dynamics with the assumption of no flow ahead of the reflected shock. The first comparison shown in figure 42 where the calculated shock fronts, the white curves, are put on top of the pictures earlier given in figure 31. We see that the shock fronts in figure 42(a) and 42(b) are completely covered by the calculated fronts and at these early stages the acoustic calculations produce a fair description of the propagation. In figure 42(c) the curvature of the corners are seen to deviate some but still the theory holds. The failure of the acoustic theory is shown in figure 42(d) where the crossing of rays occurs. The comparison with the theory based on GSD can be seen in figure 43 and shows a good agreement at all positions. We note however from the results shown in figure 32 that in the later stages a crossing of shock-shocks occurs which can not be described by the theory of geometrical shock dynamics.

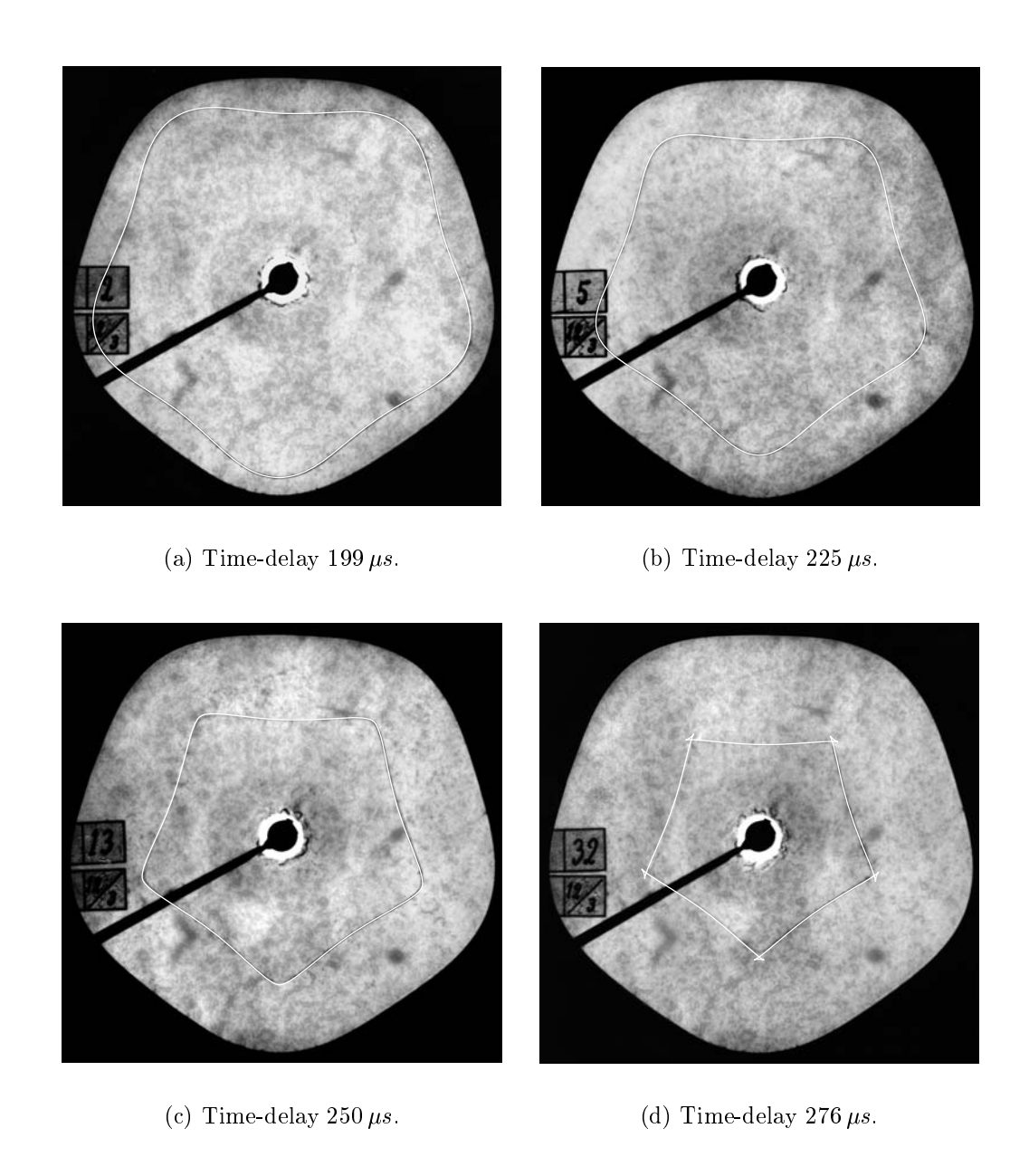


Fig. 42. The weak shock fronts compared to calculations based on geometrical acoustics, $M_0 \approx 1.1$.

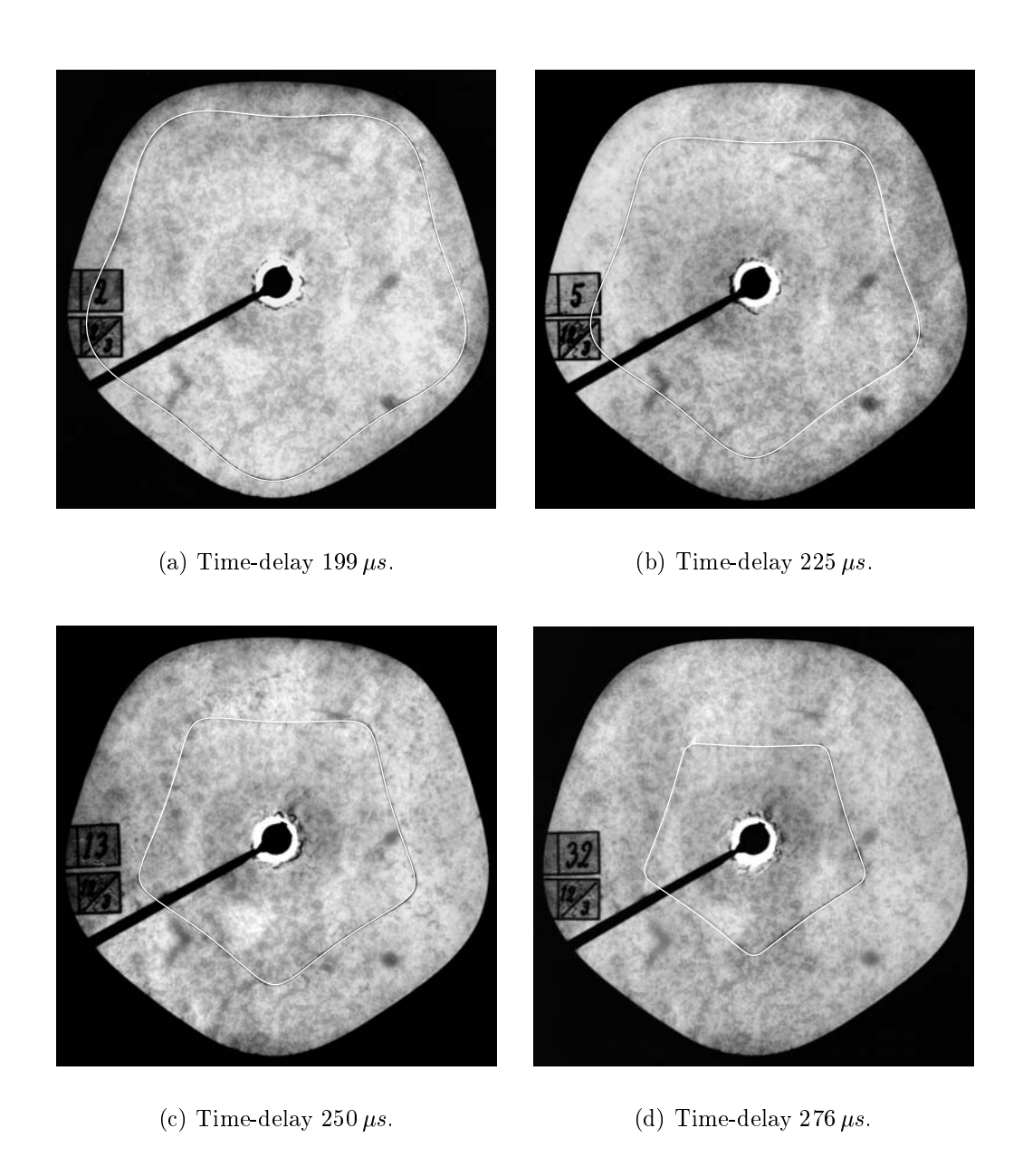
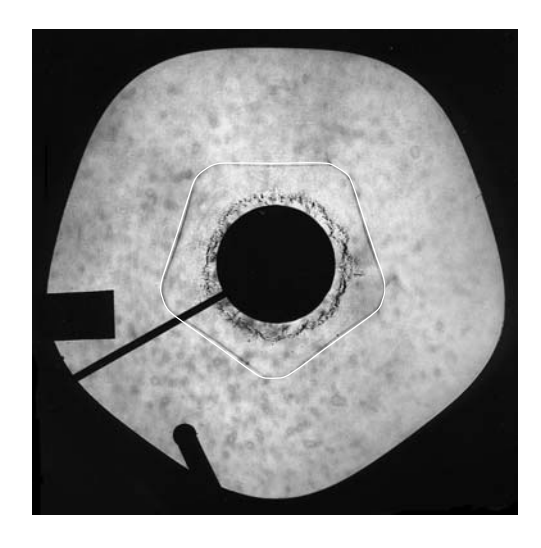


Fig. 43. The weak shock fronts compared to calculations based on geometrical shock dynamics, $M_0 \approx 1.1$.

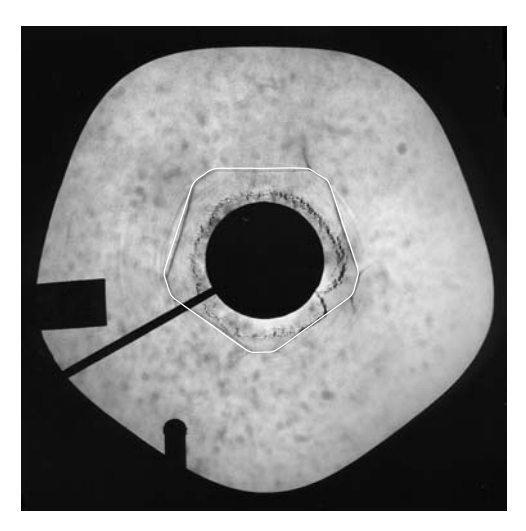
In the next comparison the results of the moderately strong experiments at the initial Mach numbers 1.35 and 1.5 are compared with two different kinds of calculations based on GSD, a calculation without a flow ahead of the reflected shock and a calculation with a linear flow ahead. Both kinds of calculations were carried out at the two Mach numbers mentioned above. The figure 44 shows the comparisons at the initial Mach number $M_0 = 1.35$: figures 44(a) and 44(b) without a flow ahead and figures 44(c) and 44(d) with the linear flow ahead. The results shows that the shock form derived from the calculations without the flow ahead gives a shock form with sides that are too straight as compared to the form found in the experimental results. On the other hand, it does describe the formation of the shock-shocks. With the linear flow ahead the shape of the sides does agree better but the corners seems to be too smooth compared to the experimental results. The same results are found in the next figure 45 where the calculations where carried out for the initial Mach number $M_0 = 1.5$. The early stages of the converging process are not shown but all the information about the deviations of the shock form for the different calculations are included in the shown results.

Which of these models that is best suited to describe the converging shock is left to the future to decide but the results shows that both methods agree well with the shock forms obtained in the present experimental study. Calculations with a flow created by a strong shock like those described in section 2 are only valid for strong shocks and results from such calculations for the above initial Mach numbers deviates too much from the experimental results.

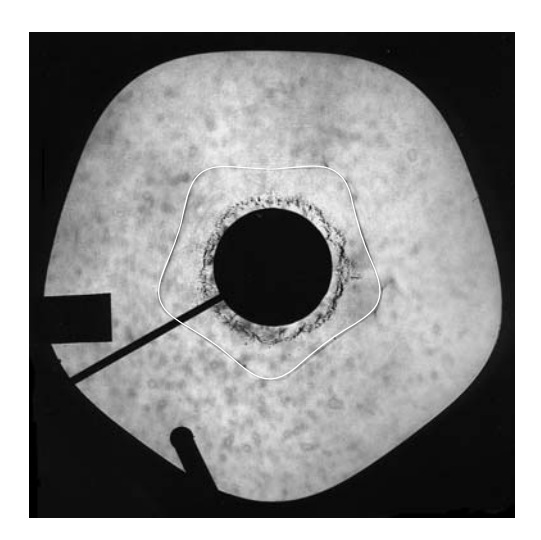
The computational model used here uses the flow behind the outward traveling shock while in the experiments we are measuring the Mach number in the reflector-fixed reference frame. Therefore a transformation of the Mach number values to this frame has to be performed in order to compare these values. There are two known analytical solutions that can be used in this respect. One which is valid for large Mach numbers. At another extreme we have the acoustic wave solution which is valid for $M \to 1$. Neither of these is quite appropriate in our intermediate case. It might be therefore of interest to use the present experimental data in order to find an appropriate model for a flow behind a shock in this intermediate case. The figure 46 shows the comparison of the calculated values with the experimental results for the initial Mach number $M_0 \approx 1.5$.



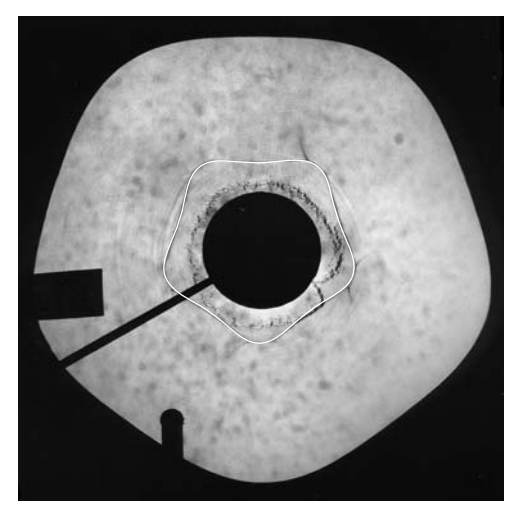
(a) Calculations without flow ahead of the shock. Time-delay 229 μs .



(b) Calculations without flow ahead of the shock. Time-delay 240 μs .

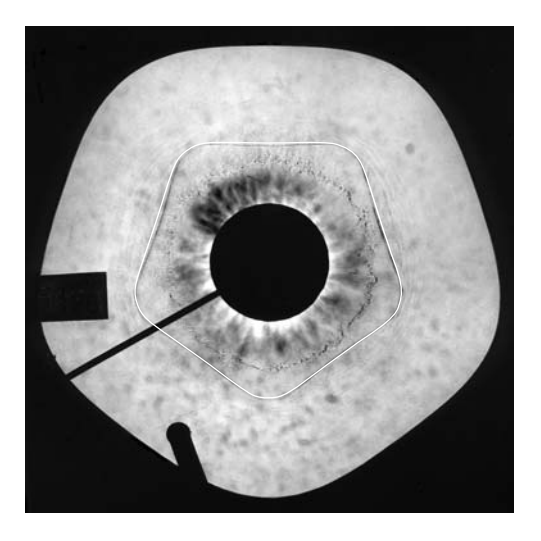


(c) Calculations with linear flow ahead of the shock. Time-delay 229 $\mu s.$

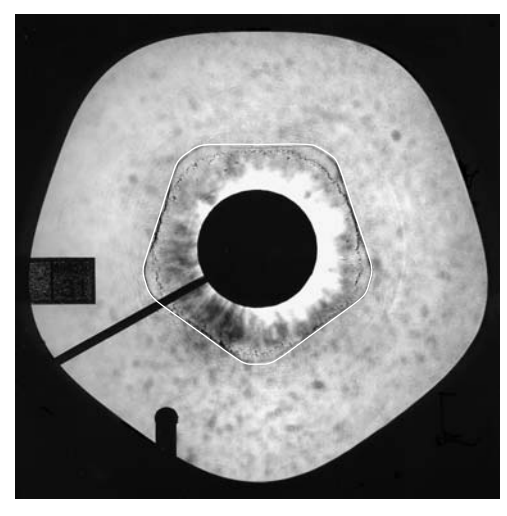


(d) Calculations with linear flow ahead of the shock. Time-delay 240 $\mu s.$

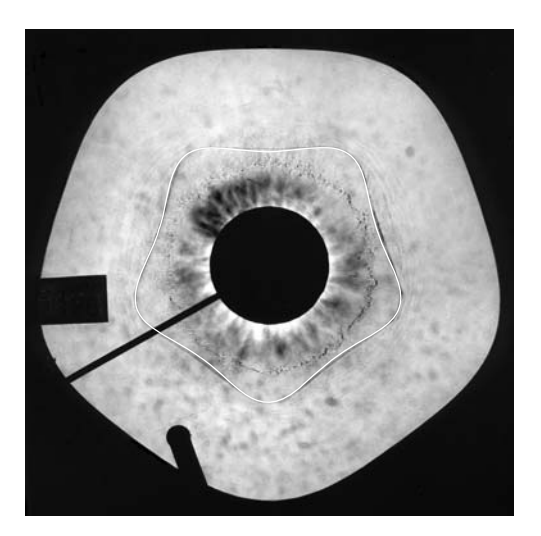
Fig. 44. The moderately strong shock fronts compared to calculations based on geometrical shock dynamics, $M_0 \approx 1.35$.



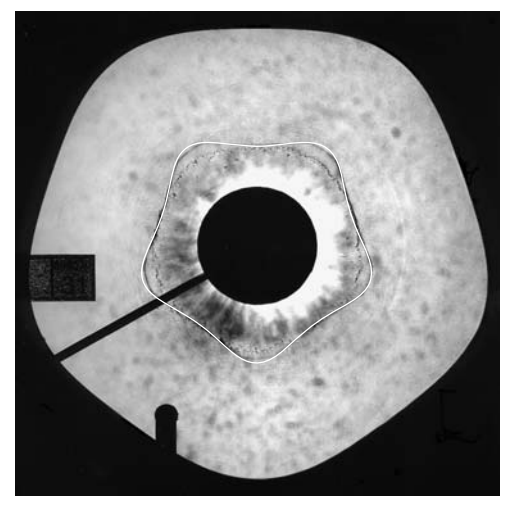
(a) Calculations without flow ahead of the shock. Time-delay $180\,\mu s$.



(b) Calculations without flow ahead of the shock. Time-delay 192 μs .



(c) Calculations with linear flow ahead of the shock. Time-delay 180 μs .



(d) Calculations with linear flow ahead of the shock. Time-delay 192 μs .

Fig. 45. The moderately strong shock fronts compared to calculations based on geometrical shock dynamics, $M_0 \approx 1.5$.

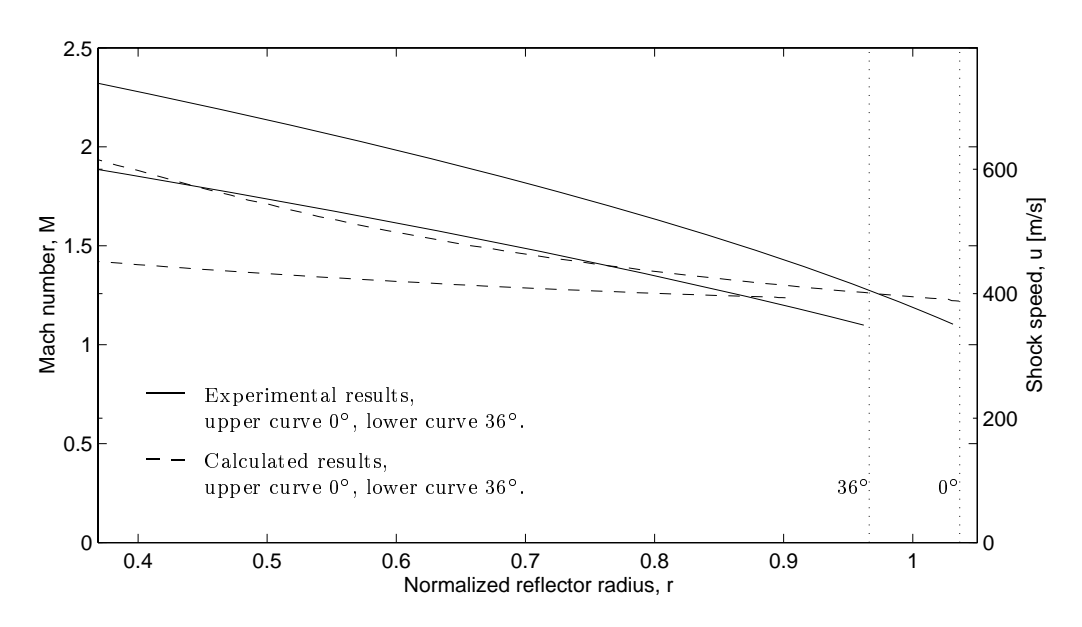


Fig. 46. Comparison of the Mach number presented in the chamber fix system, $M_0 \approx 1.5$.

5 Summary of the major results

- The major new result of the present study is the construction and test of the experimental set-up for the study of shock generation, propagation and convergence in a confined chamber of a special form. The set-up involves shock generation by means of an electrical discharge. This method is based on two different techniques an igniting spark technique as well as exploding wire method to generate the initial circular cylindrical shock in the chamber. The visualization is performed by means of the schlieren optics and the shock speed measurements by means of a HeNe laser system.
- This specific reflector form has been chosen deliberately since the shock behaviour in the corner regions of the resulting reflected shock possesses all the major features of the focusing process in general. These involves evolution of curved shock fronts to planar, creation of corners with very high curvature which leads to higher speed of shock propagation of these regions and further evolution of the shock form accordingly. All these features have been observed and investigated experimentally in the present study.
- The shocks produced in the current experiment were in the range weak $(M \approx 1.1)$, to moderately strong $(M \approx 1.7)$. The earlier theoretical studies of this problem have been compared with the present experimental results. It was shown that the predictions of the acoustic theory agreed well with the observed shock form in the case of weak shocks. It is important to note here that this agreement is satisfactory only in the early stages of the shock convergence even in the case of weak shocks. It has been shown that the acoustic theory is no longer able to describe the shock behaviour in the case of moderate and moderately strong shocks. In this case the nonlinear theory of geometrical shock dynamics has to be used. Comparison of the shock forms obtained from the calculations based on the extended form of this theory showed a good agreement with the present experimental results.
- The experimental procedures described in the above proved to be a simple, stable, repeatable and reliable methods to produce highly symmetrical polygonal-shaped converging shocks. It was shown to be possible to generate shock waves with sharp corners and plane sides by means of the reflection process off a smooth boundary having the form of a slightly perturbed circle. This is a non-trivial result since there is no obvious simple way to obtain this type of shock form.

Acknowledgements

The present investigation was initiated by Prof. Martin Lesser. His continuous support of this project and many helpful suggestions and discussions are gratefully acknowledged. I would like to thank Prof. Henrik Alfredsson for his enthusiasm and for making the excellent facilities of the Department of Mechanics laboratory available. Special thanks are due to Dr. Nils Tillmark for his helpful advice and assistance in the arrangement of the experimental set-up. I would also like to thank Mr. Marcus Gällstedt for his precision work in manufacturing the experimental apparatus and to him and Mr. Ulf Landén for their help in practical matters. Many thanks are due to my supervisor Dr. Nicholas Apazidis for support, encouragement and help in all situations that occurred. This work has been funded by TFR, the Swedish Research Council for Engineering Sciences, which is gratefully acknowledged.

References

ANDERSON J.D. 1990 Modern compressible flow. McGraw-Hill Publishing Company.

APAZIDIS N. 1992 Control of pressure distribution in shock generators with elliptic cross-section. Shock Waves Intl J. 2, 147-156.

APAZIDIS N. & LESSER M.B. 1996 On generation and convergence of polygonal-shaped shock waves. *J. Fluid Mech.* **309**, 301-319.

GUSTAFSSON G. 1985 Propagation of weak shock waves in an elliptical cavity. Doctoral Thesis, Lule University of Technology.

GUSTAFSSON G. 1987 Focusing of weak shock waves in an slightly elliptical cavity. J. Sound Vib. 116, 137-148.

HENSHAW W.D., SMYTH N.F. & SCHWENDEMAN D.W. 1986 Numerical shock propagation using geometrical shock dynamics. *J. Fluid Mech.* **171**, 519-545.

JOHANSSON B., APAZIDIS N. & LESSER M.B. 1999 On shock waves in a confined reflector. Wear 233-235, 79-85.

LIEPMANN H.W. & ROSHKO A. 1957 *Elements of gasdynamics*. John Wiley & Sons Inc.

SCHWENDEMAN D.W. & WHITHAM G.B. 1987 On converging shock waves. *Proc. R. Soc. Lond.* A **413**, 297-311.

STURTEVANT B. & KULKARNY V.A. 1976 The focusing of weak shock waves. J. Fluid Mech. 73, 651-671.

WHITHAM G.B. 1957 A new approach to problems of shock dynamics. Part1. Two-dimensional problems. J. Fluid Mech. 2, 145-171.

WHITHAM G.B. 1959 A new approach to problems of shock dynamics. Part2. Three-dimensional problems. *J. Fluid Mech.* **5**, 369-386.

WHITHAM G.B. 1968 A note on shock dynamics relative to a moving frame. *J. Fluid Mech.* **31**, 449-453.

WHITHAM G.B. 1974 Linear and nonlinear waves. John Wiley & Sons Inc.